Quantitative testing of bedrock incision models for the Clearwater River, NW Washington State

Jonathan H. Tomkin,[1,2] Mark T. Brandon,[1] Frank J. Pazzaglia,[3] Jonathan R. Barbour,[1] and Sean D. Willett[4]

Received 1 August 2001; revised 19 December 2002; accepted 13 February 2003; published 20 June 2003.

[1] The incision of rivers in bedrock is thought to be an important factor that influences the evolution of relief in tectonically active orogens. At present, there are at least six competing models for incision of bedrock rivers, but these models have received little quantitative testing. We statistically evaluate these models using observations from the Clearwater River in northwestern Washington State, which crosses the actively rising forearc high of the Cascadia margin. A previous study has used fluvial terraces along the Clearwater to estimate bedrock incision rates over the last ~150 kyr. They show that incision rates have been steady over the long-term (>50 kyr), consistent with other evidence based on isotopic cooling ages, for steady long-term (>1 Myr) erosion rates. The steady state character of the river allows us to use the relatively simple time-invariant solutions for the various incision models and also to estimate long-term sediment discharge along the river, which is a critical variable for some incision models. An interesting feature of the Clearwater River is that it has a downstream decrease in the rate of incision, from ~0.9 mm/yr in the headwater to <0.1 mm/yr at the coast. None of the incision models, including the shear stress model, successfully accounts for this relationship. This result may be due to the simple way in which these models are used, commonly without consideration for the distribution of discharge with time, and the variable capacity of the river channel to contain peak flows along its course. We suggest some general improvements for the incision models, and also guidelines for selecting those rivers that will allow good discrimination between competing models. *INDEX TERMS:* 1620 Global Change: Climate dynamics (3309); 1815 Hydrology: Erosion and sedimentation; 1824 Hydrology: Geomorphology (1625); *KEYWORDS:* landscape evolution, topography, geomorphology, erosion, incision, rivers

Citation: Tomkin, J. H., M. T. Brandon, F. J. Pazzaglia, J. R. Barbour, and S. D. Willett, Quantitative testing of bedrock incision models for the Clearwater River, NW Washington State, *J. Geophys. Res.*, *108*(B6), 2308, doi:10.1029/2001JB000862, 2003.

1. Introduction

[2] Rivers play a central role in the formation of many landscapes. They are responsible for a wide variety of landscape morphologies, such as hillslope gradient and the distribution of elevation [*Strahler*, 1964]. They set a limiting constraint upon sediment transport. River incision into bedrock also has an important influence on orogenic evolution as it links topography to tectonics and climate.

[3] In the last few years, much work has focused on understanding the process of river incision [e.g., *Bull*, 1979, 1991; *Seidl and Dietrich*, 1992; *Howard et al.*, 1994; *Kooi and Beaumont*, 1996; *Tinkler and Wohl*, 1998; *Whipple et al.*, 2000]. Despite this effort, the processes by which mountain rivers cut into bedrock remains poorly understood. Important processes may include sediment abrasion, cavitation, knickpoint propagation, plucking, and mass wasting by debris flows [e.g., *Howard et al.*, 1994; *Sklar and Dietrich*, 1998; *Whipple et al.*, 2000]. These diverse processes have inspired a variety of quantitative models to represent bedrock river incision. Our goal is to differentiate between these various models using appropriate data sets.

[4] Published incision models can be viewed as falling between two end-members. At one end of the spectrum are those models where incision is transport limited, in that incision rate is controlled by transportation of sediment through the channel [e.g., *Chase*, 1992; *Willgoose et al.*, 1991]. At the other end are those models that are production limited, in that the incision rate is limited by the rate of

[1]Department of Geology and Geophysics, Yale University, New Haven, Connecticut, USA.
[2]Now at Department of Geology and Geophysics, Louisiana State University, Baton Rouge, Louisiana, USA.
[3]Department of Earth and Environmental Sciences, Lehigh University, Bethlehem, Pennsylvania, USA.
[4]Department of Earth and Space Sciences, University of Washington, Seattle, Washington, USA.

0148-0227/03/2001JB000862$09.00

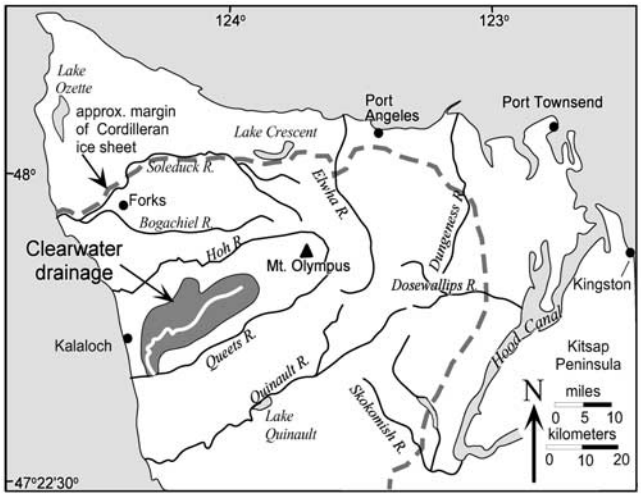

Figure 1. Location of the Clearwater River and associated drainage [from *Pazzaglia and Brandon*, 2001] (Reprinted by permission of the *American Journal of Science*.)

detachment of rock from the bedrock channel and is independent of the sediment discharge [e.g., *Seidl and Dietrich*, 1992; *Howard et al.*, 1994; *Tucker and Slingerland*, 1994]. In either case, incision rate is usually linked to the basal shear stress or stream power [e.g., *Beaumont et al.*, 1992; *Seidl and Dietrich*, 1992; *Howard et al.*, 1994; *Tucker and Slingerland*, 1994; *Slingerland et al.*, 1997, 1998] although more physically prescriptive models have also been proposed [*Sklar and Dietrich*, 1998, 2001].

[5] This study assesses the ability of different incision models to predict the rate of valley incision in the Clearwater River, which is located in the Olympic Mountains of NW Washington State. *Pazzaglia and Brandon* [2001] identify two major straths preserved along much of the length of the trunk channel of the Clearwater. These straths were buried at ~65 and ~140 *ka*. Thus the heights of these different straths provide two independent sets of incision rates for the Clearwater. The fact that these rates are similar indicates that bedrock incision has been occurring at a relatively steady pace on a 50 kry timescale [*Pazzaglia and Brandon*, 2001]. This result means that long-term sediment discharge along the course of the river can be estimated. This information is important for testing models that are dependent on sediment discharge. In this study, we discriminate between competing incision models by using standard inversion methods and statistical tests.

[6] In our analysis, none of the models examined, including the popular "stream power" model, successfully explain the observed incision rates of the Clearwater River. The models provide reasonable descriptions of the physics of incision. Thus we suspect that the difficulties of the models to fit the Clearwater incision data may be due to the way they are implemented, and not to the physical principles on which they are based. We discuss this issue and suggest ways that the models might be modified to better represent long-term incision in real rivers.

2. The Clearwater River

[7] The Clearwater River (Figures 1, 2, and 3) occupies a relatively large drainage, 390 km^2, with elevations ranging

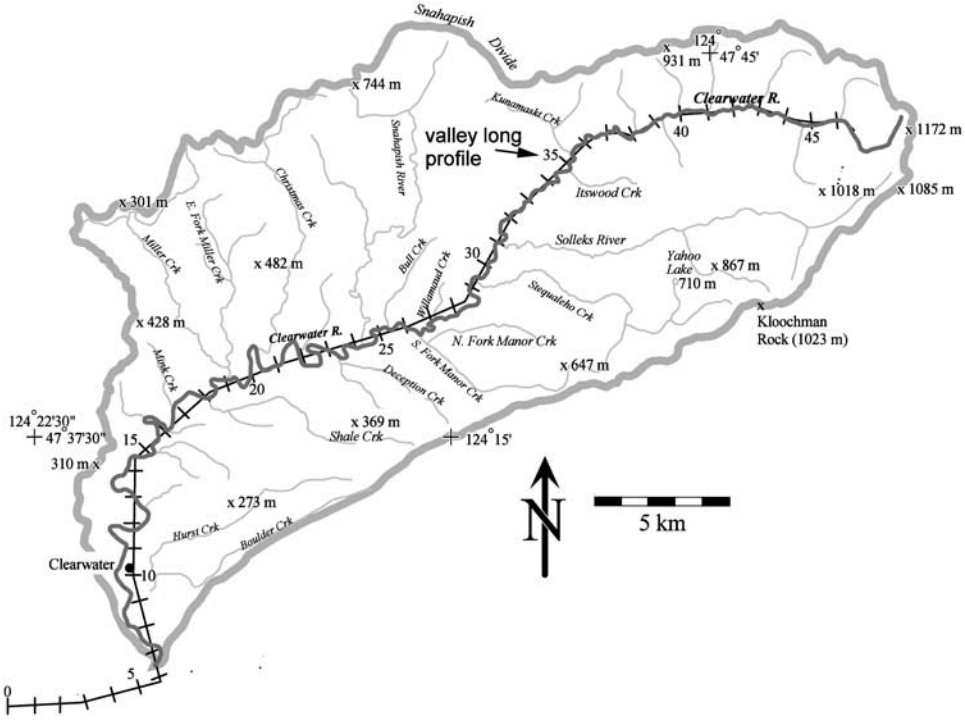

Figure 2. Map of the Clearwater drainage [from *Pazzaglia and Brandon*, 2001]. The scaled line shows valley distance in kilometers along the axis of the Clearwater valley. (Reprinted by permission of the *American Journal of Science*.)

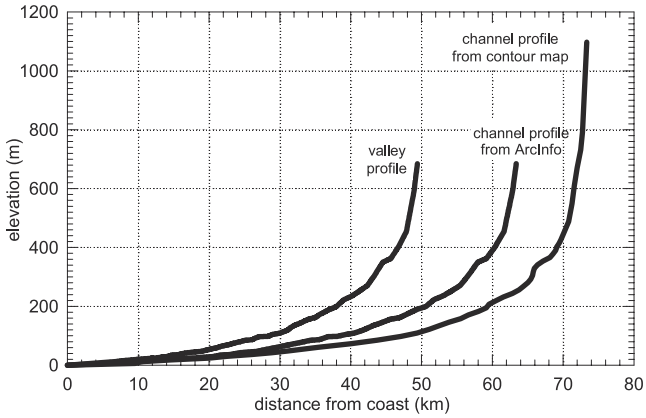

Figure 3. Long profiles of the Clearwater River. The valley profile indicates a profile relative to valley distance, as defined in Figure 2. The channel profiles are shown relative to the distance along the main channel, as determined by ARCINFO analysis of digital elevation data or by manual measurements from a 7.5′ topographic map. The difference between the two channel profiles is due to the fractal geometry of the channel in map view.

from 12 m to 1130 m. Precipitation ranges from about 250 cm/yr. at the mouth of the drainage to 400 cm/yr in the headwaters. The drainage is underlain by a homogeneous assemblage of indurated sandstone with minor shale interbeds [*Tabor and Cady*, 1978], minimizing rock type as a geomorphic variable. Schmidt hammer measurements indicate a compressive strength for the sandstones of ~40 N/mm^2 (range 12 to 56 N/mm^2 for 27 measurements) and for mudstones and fine sandstones of ~23 N/mm^2 (range 12 to 38 N/mm^2 for 5 measurements). The trunk channel of the Clearwater contains a mix of alluvial and bedrock reaches. The amount of alluvial cover increases downstream, but it is almost everywhere less than 3 m, a thickness that can be easily transported during high flow conditions. On a slope-area plot (Figure 4), the lower Clearwater plots in the alluvial field of *Montgomery et al.* [1996]. However, *Pazzaglia and Brandon* [2001] demonstrate that the river is incising into bedrock along its entire length.

[8] The river seems to have maintained a steady base level, even in the present of major changes in sea level [*Pazzaglia and Brandon*, 2001]. The reason is that the lower reach of the river has a gradient similar to its submerged course across the continental shelf, which means that the river sees a steady base level even as the mouth of the river migrates with the coastline. The long profile of the river lacks any evidence of large migrating knickpoints, as might be produced if eustatic variations could causes changes in base level.

[9] We use remnants of the old river channel, called straths, to measure fluvial incision [*Pazzaglia and Brandon*, 2001]. Straths are flat eroded surfaces cut into bedrock. They are found in the hillslopes above an actively incising river and are attributed to periods of time when the river was able to incise into bedrock and to cut a broad flat valley floor. The Clearwater River is currently eroding into bedrock. Thus the height of a strath above the modern river marks the amount of incision of the river channel into bedrock. Strath incision rates are shown (Figure 5e) relative to the valley long profile, which marks the course of the central axis of the Clearwater valley (Figure 2). This rate is actually a valley incision rate E_v, since it measures the long-term rate of down cutting for the entire width of the valley. The bedrock incision models are usually formulated for a channel incision rate E_c, so we need to relate E_c to E_v.

[10] There are two end-member relationships that are be considered. The first is that lateral incision on the valley floor is relatively "easy" compared to vertical incision of the channel [e.g., *Hancock and Anderson*, 2002]. In the extreme, this view would predict that the vertical incision of the channel is the rate-limiting process for the vertical incision of the valley so that E_v should be equal to E_c.

[11] The alternative end-member is channel incision is responsible for downcutting of the entire valley floor. In this case, valley incision occurs only because the river channel is considered to meander across the valley floor so that the channel erosion is not focused in one location. The long-term rate of valley incision will be slower in this case then the rate of channel incision observed over the short term. The difference in rates is given by

$$E_c W_c = E_v W_v \tag{1}$$

$$\frac{E_c}{E_v} = \frac{W_v}{W_c}. \tag{2}$$

We follow the usual procedure in which valley and channel width are considered to vary as as a power function of drainage area [e.g., *Snyder et al.*, 2001]. Channel width was measured in the field. The current width of the valley floor is well defined and measured from 7.5′ topographic maps. These data are represented by the following best fit power law equations (Figure 6):

$$W_v = 2.81A^{0.76} \tag{3}$$

$$W_c = 4.20A^{0.42}, \tag{4}$$

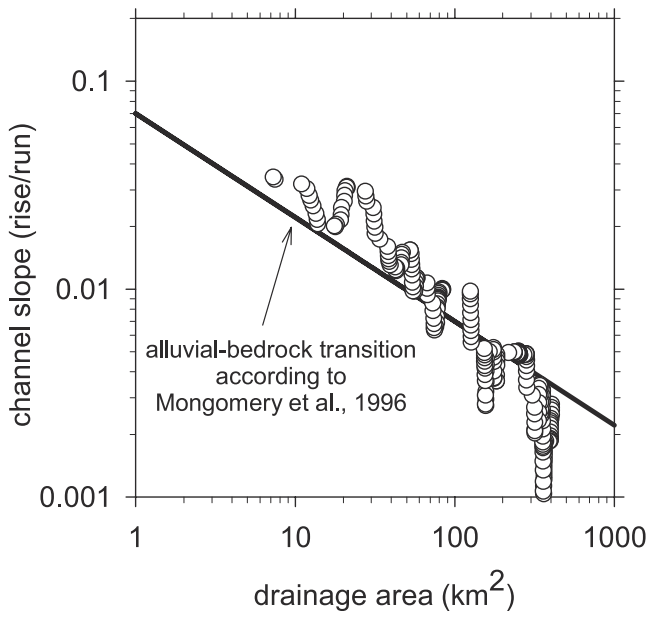

Figure 4. Slope-area plot for the Clearwater River.

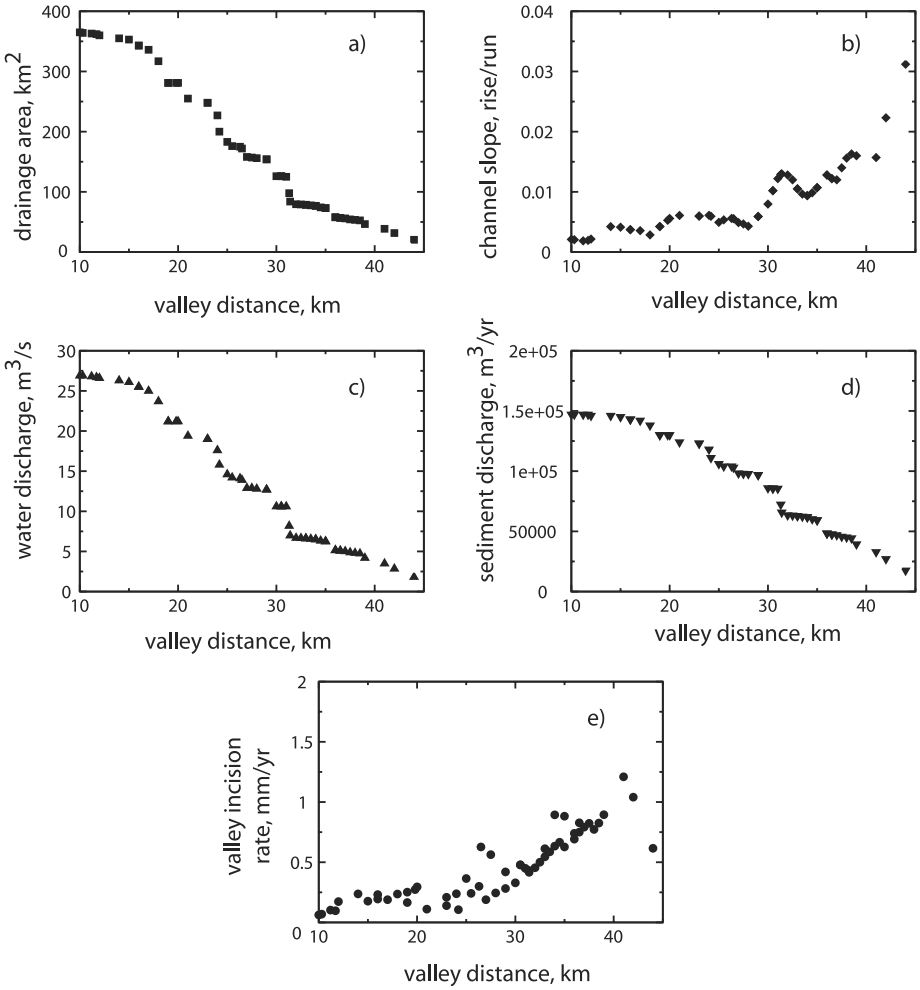

Figure 5. Data for the Clearwater River as a function of valley distance: (a) area, (b) channel slope, (c) water discharge, (d) sediment discharge, and (e) valley incision rate.

where A is in km^2 and W is in m. Discharge, Q (m^3/s) is related to area: $A = 9.37Q^{1.1}$. The incision rate ratio of the channel relative to the valley is

$$\frac{E_c}{E_v} = \frac{2.81A^{0.76}}{4.20A^{0.42}} = 0.67A^{0.34} = 1.43Q^{0.38} \quad (5)$$

[12] This relationship indicates that $E_c > E_v$ and that the difference between the two rates increases downstream as A and Q increase because the river channel widens downstream at a slower rate then the widening of the valley floor.

[13] These end-member options are important for our analysis because they change the predictions about the relationship of incision rate to upstream area A. For the statistical tests employed below, we allow for the full range of valley widening behavior, ranging from the first case where $E_c = E_v$ to the second case where E_c is a more complex function of E_v (equation (5)).

[14] Channel location, drainage area, and discharge were determined using an overland flow routine in ARCINFO. Results are reported in Figure 5 and Table 1. Topography was represented using 30-m gridded elevation data from the U.S. Geological Survey. The horizontal location of the channel determined by the ARCINFO routine compares

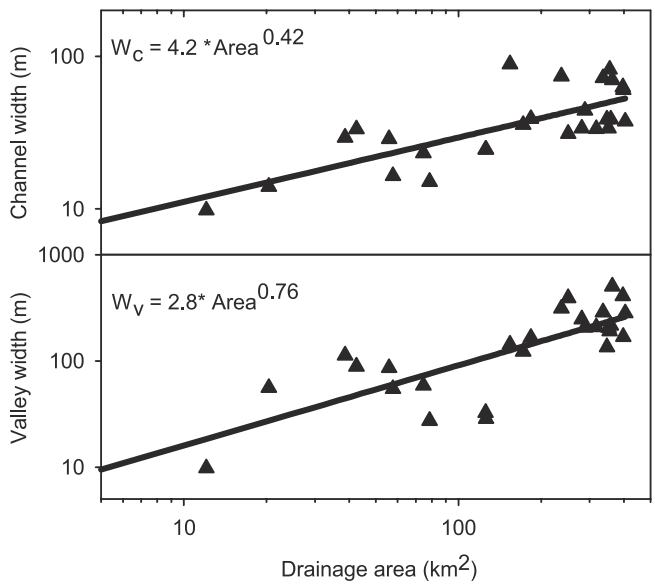

Figure 6. Channel and valley width data as a function of drainage area for the Clearwater River. Lines and equations show best fit power law equations.

Table 1. Clearwater River Data

Valley Distance, km	Channel Distance, km	Area, km^2	Channel Slope, 10^{-3}	Valley Slope, 10^{-3}	Discharge, m^3/s	Sediment Discharge, 10^4 m^3/yr	Incision Rate, mm/yr
10.0	14.0	365	1.76	2.10	26.9	14.7	0.0618
10.3	14.4	364	1.66	2.05	26.9	14.7	0.0688
11.2	15.5	363	1.34	1.86	26.8	14.7	0.102
11.7	16.0	362	1.17	1.93	26.7	14.7	0.0967
12.0	17.4	360	0.93	2.16	26.6	14.6	0.173
14.0	20.5	355	3.11	4.23	26.3	14.6	0.237
15.0	22.0	353	2.63	4.13	26.1	14.5	0.176
16.0	23.4	343	3.18	3.72	25.5	14.3	0.194
16.0	23.4	343	3.18	3.72	25.5	14.3	0.231
17.0	24.5	336	3.15	3.56	25.0	14.2	0.189
18.0	25.7	317	2.07	2.85	23.7	13.8	0.236
19.0	26.9	281	3.66	4.24	21.2	13.0	0.165
19.0	26.9	281	3.66	4.24	21.2	13.0	0.251
19.8	27.8	281	4.78	5.28	21.2	13.0	0.273
20.0	28.0	281	4.87	5.58	21.2	13.0	0.295
21.0	29.2	255	4.82	6.08	19.4	12.4	0.110
23.0	31.7	248	4.91	5.98	19.0	12.3	0.140
23.0	31.7	248	4.91	5.89	19.0	12.3	0.209
24.0	33.0	227	4.97	6.10	17.6	11.8	0.238
24.2	33.2	200	4.89	5.94	15.8	11.1	0.106
25.0	34.2	183	3.70	4.94	14.6	10.6	0.365
25.5	34.8	176	3.72	5.35	14.2	10.4	0.242
26.3	35.9	175	5.15	5.59	14.1	10.4	0.300
26.5	36.2	172	5.08	5.55	13.9	10.3	0.627
27.0	36.7	158	4.33	4.89	12.9	9.82	0.189
27.5	37.2	157	3.35	4.67	12.9	9.79	0.563
28.0	37.8	156	2.77	4.29	12.8	9.77	0.245
29.0	39.4	154	4.72	5.91	12.7	9.68	0.282
29.0	39.4	154	4.72	5.91	12.7	9.68	0.420
30.0	40.5	126	6.27	7.97	10.6	8.59	0.329
30.5	41.1	126	7.57	10.2	10.6	8.57	0.478
30.5	41.1	126	7.57	10.2	10.6	8.57	0.478
31.0	41.7	125	9.36	12.2	10.6	8.55	0.450
31.3	42.1	97.8	9.87	12.9	8.18	7.23	0.434
31.4	42.4	83.9	10.0	13.0	6.98	6.57	0.416
32.0	43.2	79.4	9.64	12.8	6.68	6.34	0.454
32.5	43.8	79.1	9.09	12.0	6.66	6.32	0.500
33.0	44.4	78.5	8.86	1.05	6.62	6.28	0.545
33.0	44.4	78.5	8.86	1.05	6.62	6.28	0.612
33.5	44.0	77.6	8.13	9.63	6.56	6.23	0.587
34.0	44.5	76.8	6.86	9.38	6.50	6.18	0.633
34.0	44.5	76.8	6.86	9.38	6.50	6.18	0.894
34.5	46.3	74.2	6.55	9.85	6.33	6.02	0.666
35.0	47.0	73.0	8.08	10.7	6.25	5.93	0.627
35.0	47.0	73.0	8.08	10.7	6.25	5.93	0.882
36.0	48.3	57.8	11.3	12.8	5.15	4.83	0.692
36.0	48.3	57.8	11.3	12.8	5.15	4.83	0.740
36.5	48.8	56.8	10.6	12.2	5.08	4.75	0.750
36.5	48.8	56.8	10.6	12.2	5.08	4.75	0.827
37.0	49.3	55.9	9.75	12.0	5.02	4.69	0.791
37.5	50.0	54.3	11.0	14.0	4.88	4.56	0.823
38.0	50.6	53.5	13.5	15.6	4.81	4.50	0.772
38.5	51.2	52.6	15.4	16.3	4.74	4.43	0.825
39.0	51.7	46.5	14.7	16.0	4.19	3.93	0.895
41.0	53.9	38.6	14.0	15.7	3.49	3.28	1.21
42.0	55.1	31.6	19.4	22.3	2.85	2.70	1.04
44.0	57.3	20.4	27.9	31.2	1.82	1.75	0.616

well with the mapped location of the river from 7.5′ USGS contour maps. Longitudinal profiles of the channel are also similar in shape (Figure 3) but the horizontal length of the ARCINFO-based profile was 15% shorter than that for the map-based profile. The fact that the two profiles are scaled equivalents is predictable given the fractal shape of the channel and the differences in scale length implicit in the map and DEM data. Channel slopes were determined by linear regression of the ARCINFO profile of elevation versus channel distance using a 3-km-long moving window (Figure 5b). The objective was to reduce the noise introduced by the discrete nature of the gridded data. The 3-km window was considered appropriate given that the individual strath measurements provided incision rates averaged over the width of the valley, which has a scale length of 100 to 300 m. The fractal shape of the channel is also a factor for the ARCINFO-based channel slopes, which are greater than those determined from contour maps by the same 15%.

[15] Figure 5 also provides other data used for our modeling, including drainage area as determined using ARCINFO, long-term incision rates from *Pazzaglia and Brandon* [2001], and sediment discharge. The sediment discharge data along the river were estimated assuming steady state incision of the river valley. *Pazzaglia and Brandon* [2001] argue that the Clearwater cut its valley at a steady rate when averaged over a long time frame (>50 kyr). *Brandon et al.* [1998] and *Batt et al.* [2001] provide other evidence that indicates that long-term erosion rates in the Olympics have been fairly steady on a 1 Myr time frame. Thus we conclude that the hillslopes are probably being lowered at the same rate that the river is incising. If correct, then the long-term sediment discharge carried by the river can be defined as a function of upstream area A using

$$q(A) = \int_0^A E_v(A')dA', \tag{6}$$

where $E_v(A')$ and $q(A)$ are the valley incision rates and sediment discharge, respectively, with the upstream drainage area A defining the location along the river (A' is a dummy variable for the integration).

[16] Discharge was determined using a gridded data set based on a 30-year precipitation record (1961–1990) (PRISM method [see *Daly et al.*, 1994, 2001]). The PRISM method interpolates precipitation from monitoring stations to grid points and takes into account variations due to slope and elevation. The gridded data are available on a mean monthly basis or a mean annual basis. The data were used to construct the density distribution for monthly precipitation shown in Figure 7. Precipitation rates vary with time, but the spatial distribution of precipitation across the Olympic (not shown) is nearly identical on a month-by-month basis. For our analysis, we use the mean annual precipitation grid, but any of the monthly grids would have sufficed given the right scaling factor for the magnitudes of the different months relative to the mean annual magnitude. Ambiguities in linear scaling factors (such as this one) are accounted for in our analysis below. As presently formulated, most models do not require an explicit definition of the effective discharge. There is one class of models that does, those that propose that incision does not start until the discharge exceeds a threshold value [*Howard*, 1997; *Tucker and Slingerland*, 1997]. Such models are sensitive to the actual distribution of discharge in the channel, as considered below.

[17] Discharge represents only that portion of precipitation that reaches the river channel. A significant volume of water is lost to evaporation from vegetation, soil, and water bodies [*Leopold*, 1994]. Evapotranspiration data were obtained from the U.S. Bureau of Reclamation [*USDA-*

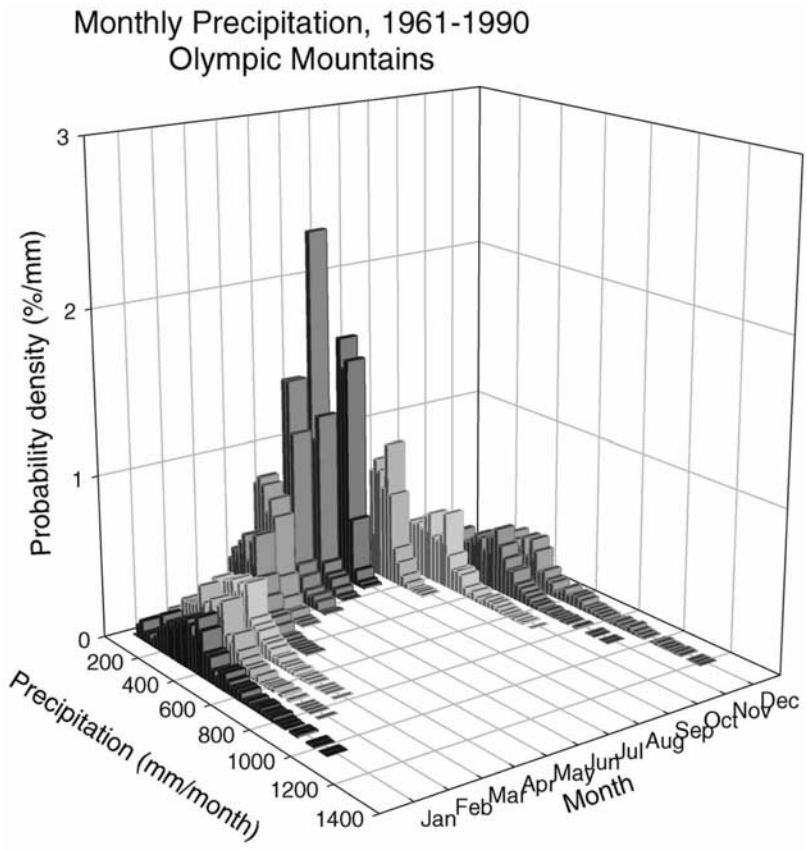

Figure 7. Area distribution for mean monthly precipitation rates for the Olympic Peninsula.

NRCS, 1998] for two nearby sites in the Oregon-Washington Coast Ranges for the 1961–1990 period represented by the PRISM data set. Evapotranspiration was 0.85 m/yr for Bandon, Oregon, and 1.2 m/yr for Corvallis, Oregon. We took the average, 1 m/yr, as representative for the Olympics. This value was subtracted from each cell of the precipitation grid. The few cells with <1 m/yr of precipitation were set to zero. The resulting annual precipitation was then routed over the landscape to create a discharge grid. River channels were easily distinguished by areas with high discharge (>0.01 m^3/s). *Barbour* [1998] did this calculation for the entire Olympic Peninsula. He tested the accuracy of the discharge grid by comparison with local discharge measurements at seven gauging stations around the Olympics, including one from the lower part of the Queets River (the Clearwater River drains though that part of the Queets). The ARCINFO estimates were routinely higher than the mean annual discharge measured at the gauging stations, by about 10 to 20%. This error could be due to a slight underestimate of the evapotranspiration correction.

[18] Area A is often used as a substitute for Q and W_c as these terms are observed to scale approximately with A according to power laws:

$$Q = k_Q A^c \tag{7}$$

$$W_c = k_w Q^b = k_w k_Q^b A^{bc}, \tag{8}$$

where c is ~1 [*Dunne and Leopold*, 1978] and b is ~0.5 [*Leopold and Miller*, 1956]. For the Clearwater the power relationship between A (km^2) and Q (m^3/s) is described by $k_Q = 0.1335$ and $c = 0.90$. Using equations (4) and (7), we can calculate the power law relationship between W_c (m) and Q (m^3/s) with $k_w = 10.82$ and $b = 0.47$.

[19] The distribution of grain size along the river is shown in Figure 8, with the symbols indicating the median size and the bars indicating the 95% range. Clast-size distributions were measured in channel fill deposits preserved in Holocene and late Pleistocene terrace fill units of the Clearwater (symbols identify sites by unit and position in the terrace fill sequence; see caption for details). We emphasize that these measurements provide a record of channel grain size that spans the same duration as the incision record provided by the strath data. At each site, more than 100 clasts were selected at random using a volleyball net to provide uniform sample locations. The important observation is that grain size does not vary significantly downstream. As a result, our modeling of the Clearwater can ignore this variable.

[20] The chief feature of the data set is a strong correlation of increasing slope with increasing incision rate (Figure 9a) and a similar correlation of increasing area with decreasing incision rate (Figure 9b). It should be remembered that slope and area characteristically vary together (Figure 4) and the correlations in Figure 9 do not indicate causation.

3. Proposed River Incision Models

[21] In this section, the models and their parameterizations are outlined. We focus specifically on the functional forms of various incision models. This approach is useful

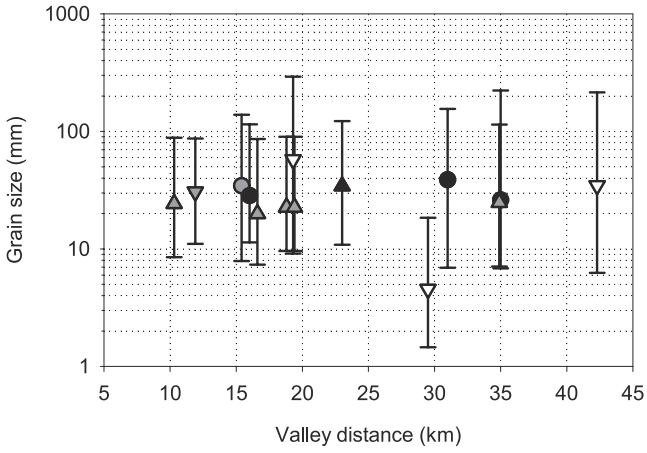

Figure 8. Grain-size distribution as a function of valley distance for 14 sites along the Clearwater River. The main conclusion is that median grain size does not change significantly downstream. The symbols indicate the median grain size (D_{50}) at each site, and the range indicates the 95% interval around the median. See text for details about how data were collected. Symbol fill indicates the age of the sampled deposit according to *Pazzaglia and Brandon* [2001]: white, 4–8 ka (QT5 deposit); gray, 65–60 ka (QT3 deposit); black, 140–135 ka (QT2 deposit). Shape of symbol indicates position in terrace deposit: bottom, inverted triangle; middle, circle; top, triangle.

because it allows entire classes of models to be evaluated, enabling broad statements to be made about the viability of the models. Our statistical tests below focus on best fit values for those parameters most diagnostic of the incision processes represented by the models. In particular, we focus on estimates on ν and μ, which represent exponents for channel slope and normalized discharge (e.g., S^{ν} and $(Q/W_c)^{\mu}$). Note that we have substituted ν and μ instead of the usual exponent variables n and m. This has been done to emphasize that our analysis is based not on area A but rather on normalized discharge, as indicated by Q/W_C. The models contain other fit parameters, but their estimated values are specific to features in the local setting, such as rock strength and discharge characteristics, and do not help in comparison of the models.

[22] An important test is to see if the best fit solution for each of the models includes physically plausible estimates for ν and μ. An extreme example would be a model that yielded estimates for ν or μ of less than zero, which would imply that a decrease in channel slope or a decrease in normalized discharge would cause an increase in incision rate. These estimates make no physical sense and thus would be strong evidence against the model as presently formulated. There are numerous predictions in the literature, which we summarize below, about what μ and ν should be for specific erosion processes. These predictions can be used to assess the validity of the fit estimates. However, it is important to remember that the published predictions for these parameters are based on simplifying assumptions, which have yet to be carefully assessed. Furthermore, the models themselves may not be correctly implemented to represent long-term incision in real rivers. We have already discussed an example of this problem above, when we considered how the long-term incision rate of the valley, as represented by the strath data in the Clearwater, might be related to the rate of channel incision. Thus our tests here focus on the performance of the models as they are currently implemented. Subsequent discussion considers how the models might be improved.

[23] The models tested here fall into three broad categories: production-limited incision (models 1, 3, and 4), transport-limited incision (model 5), and a mixture of the two (model 2, 2a, and 6).

3.1. Model 1: Shear Stress Incision

[24] *Howard and Kerby* [1983], *Seidl and Dietrich* [1992], and *Howard et al.* [1994], among others, have proposed that the bedrock incision rate of a river is proportional to the basal shear stress in the river. This model is formulated using basal shear stress but it is functionally equivalent to the "unit stream power" model, as noted by *Whipple and Tucker* [1999].

[25] The volume of bedrock eroded per unit area of channel per unit time is given by

$$E_c = k_b \tau_b^a, \tag{9}$$

where k_b is a dimensional coefficient with a value that depends on the dominant erosion process and rock strength,

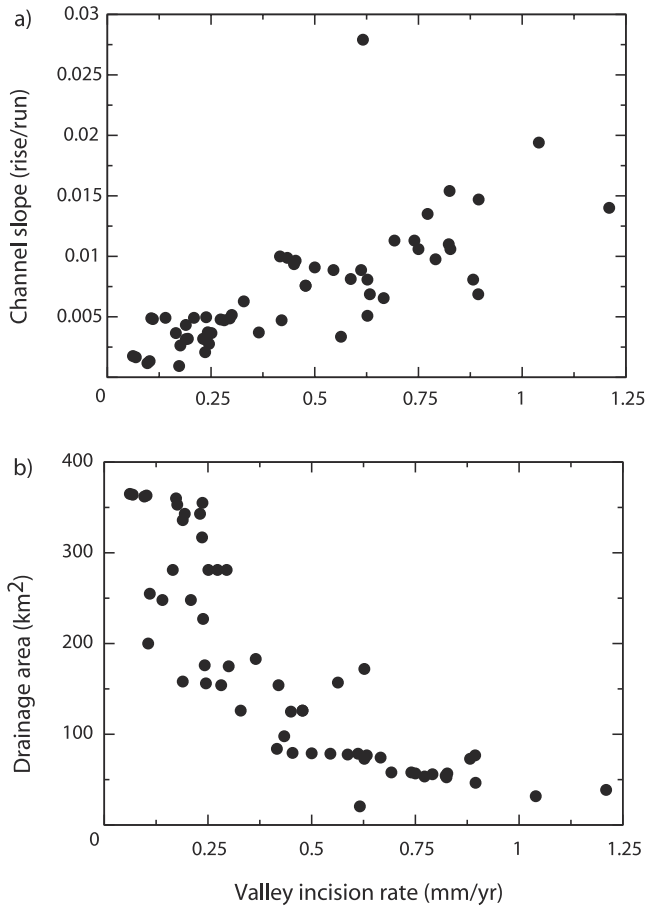

Figure 9. (a) Channel slope versus valley incision rate, and (b) drainage area versus valley incision rate for the Clearwater River.

τ_b is the basal shear stress, and a is a positive constant. a may range from around 1 for an easily eroded material [*Howard and Kerby*, 1983], to around 5/2 for impact abrasion [*Hancock et al.*, 1998].

[26] For a steady, uniform flow, the basal shear stress is given by

$$\tau_b = \rho_w k_f^{\frac{1}{3}} \left(\frac{gSQ}{W_c} \right)^{\frac{2}{3}}, \tag{10}$$

where ρ_w is the density of water, k_f is a dimensional coefficient, g is the acceleration due to gravity, Q is the steady discharge, S is the channel gradient, and W_c is the channel width [*Howard and Kerby*, 1983].

[27] The incision rate may therefore be described as

$$E_c = k_1 S^{\nu} \left(\frac{Q}{W_c} \right)^{\mu}, \tag{11}$$

where

$$k_1 = k_b \left(k_f^{\frac{1}{3}} \rho_w g^{\frac{2}{3}} \right)^a, \tag{12}$$

$$\nu = \mu = \frac{2a}{3}. \tag{13}$$

In practice, there is no general prediction for k_1, but μ and ν are predicted to be approximately equal and confined to the range 2/3 to 5/3 [*Hancock et al.*, 1998; *Whipple et al.*, 2000].

[28] As discussed above, there is an uncertainty about how E_c described by the incision models is related to E_v as determined from the strath data. The two end-member possibilities are that $E_c = E_v$ and that $E_c = 1.43\ E_v Q^{0.38}$ (equation (5)). We can substitute the second expression into equation 11 to expand the predicted range to include these two end-member options. This is discussed further in section 4.2.

3.2. Model 2: Under-Capacity Incision

[29] In this model, the sediment-carrying capacity of a river is considered to be proportional to basal shear stress [*Armstrong*, 1980; *Begin et al.*, 1981]. This concept has been used to formulate a bedrock incision model [*Chase*, 1992; *Beaumont et al.*, 1992; *Kooi and Beaumont*, 1996] in which bedrock incision is related to the amount of basal shear stress available above that needed to transport the ambient sediment discharge. The incision rate is assumed to decrease linearly with increasing sediment discharge. The incision rate becomes zero where the sediment discharge matches the maximum "carrying capacity" of the river.

[30] This model is formulated by *Beaumont et al.* [1992] as

$$E_c = c_0 S^{\nu} Q^{\mu} - c_1 q. \tag{14}$$

where c_0 and c_1 are positive constants and q is the sediment discharge (the total local sediment load of the river). They set μ and ν equal to 1, but these parameters could range more widely. We also test a variant of this model that accounts for the change in channel width downstream, as in model 1. This variant, which we designate as model 2a, is given by

$$E_c = c_0 S^{\nu} \left(\frac{Q}{W_c} \right)^{\mu} - \frac{c_1 q}{W_c} \tag{15}$$

In this form, the under-capacity model is now given in terms of excess basal shear stress, so the formulation parallels that used in model 1. The predicted values of ν and μ are the same as those for model 1, for the same reasons outlined there.

3.3. Model 3: Sediment-Limited Incision

[31] As originally hypothesized by *Gilbert* [1877], sediment discharge may influence the rate of bedrock erosion through two opposing mechanisms: (1) sediment provides tools for bed abrasion and (2) sediment protects the bedrock by reducing exposure to the erosional flow. This hypothesis has seen renewed attention from *Sklar and Dietrich* [1998, 2001], We attempt a test of Gilbert's hypothesis using parabolic equation to represent the effects of sediment discharge and basal shear stress on incision rate. *Tucker and Whipple* [2002] use a similar approach. In models 1 and 2, the higher the basal shear stress, the higher the rate of incision. The key feature of the model here is that incision rate is maximized for certain values of sediment discharge and basal shear stress.

[32] Consider first the role of sediment discharge by fixing the basal shear stress as constant. At low sediment discharge, the incision rate is controlled by the availability of tools and thus incision becomes more rapid as sediment discharge increases. However, as bed coverage increases the bed becomes shielded, decreasing the ability of the tools to work on the bedrock channel. Incision rate therefore reaches a maximum and then returns to zero as sediment discharge increases. Further increases in sediment discharge will cause aggradation and the formation of an alluvial channel.

[33] Consider now the role of changing basal shear stress at a constant sediment discharge. Basal shear stress is linked to the incision rate through two opposing mechanisms: (1) it represents the force per unit area available to abrade the bed, and (2) it controls the entrainment of sediment in the flow and thus the frequency of particle/bed impacts. As the basal shear stress increases, the tools become more energetic and are more effective at abrading the bed. The frequency of tool impacts is reduced, however. This effect eventually outweighs the increased abrasion caused by having higher energized tools and results in the incision rate falling as the shear stress increases beyond a maximum value [see *Sklar and Dietrich*, 1998, Figure 12].

[34] In an attempt to represent this model with a minimum of free parameters, we propose the following relationship:

$$E_c = \left[\left(S^{\nu} \left(\frac{Q}{W} \right)_c^{\mu} \right) - d_2 \left(S^{\nu} \left(\frac{Q}{W} \right)_c^{\mu} \right)^2 \right] \cdot \left(c_1 \frac{q}{W_c} - c_2 \frac{q^2}{W_c} \right), \tag{16}$$

where c_1, c_2, and d_2 are positive constants (note that no constant K or c_0 is required as it is made redundant by the other constants here). The defining concept of this model is

that there is both an optimum sediment load and an optimum basal shear stress.

[35] Our formulation neglects downstream changes in grain size. As the grain size does not change appreciably downstream in the Clearwater (Figure 8), this effect is unimportant for our analysis here. The expectation for *Sklar and Dietrich*'s [1998] sediment limited model is that ν and μ should both be approximately 1. Although we are testing a different sediment-limited model, we anticipate similar values. It will be shown in the results section that the exact predictions of ν and μ values are not needed.

3.4. Model 4: Shear Stress Incision With Threshold

[36] This model is detachment-limited in that the river must produce a critical basal shear stress τ_c to detach pieces of the bedrock channel [*Howard*, 1997; *Tucker and Slingerland*, 1997]. This model is described by

$$E_c = k_b(\tau_b - \tau_c)^a. \tag{17}$$

We replace τ_c with an adjustable constant below, and rewrite the equation so that it can clearly test this threshold model:

$$E_c = k_1\left(\frac{SQ}{W_c} - b_0\right)^{\nu}, \tag{18}$$

where b_0 is a constant related to the critical basal shear stress. In model 1, we noted that the basal shear stress formulation predicts that $\nu = \mu$ and that a is proportional to these exponents. Thus model 4 shows only one exponent parameter, ν, and thus prescribes that $\nu = \mu$. The predictions for ν and μ are the same as those for model 1, for the same reasons outlined above.

3.5. Model 5: Transport-Limited Stream Power Incision

[37] In a rapidly uplifting terrain, the rate-limiting aspect for incision of the channel may be the removal of eroded materials. This represents a case in which channel incision is limited by transport processes, rather than by processes that break down and detach material from the bedrock channel. If the incision rate is transport limited rather than detachment limited, one might propose that sediment discharge is controlled by the basal shear stress [*Willgoose et al.*, 1991]

$$q = K_T S^{\nu}\left(\frac{Q}{W_c}\right)^{\mu+1} \tag{19}$$

where K_T is a transport coefficient and ν and μ are positive constants.

[38] As q is the product of integrated erosion of the upstream catchment (equation (6)), we can differentiate the above with respect to area to obtain an erosion rate. If we use equation 4 ($W_c \propto A^{0.42}$) and use the fact that Q is approximately linear with respect to A (equation (12)), we then have

$$E_c = K(\mu+1)S^{\nu}(Q)^{0.58(\mu+1)-1}, \tag{20}$$

where K is a constant.

Table 2. Model Functional Forms

Model	Functional Form
1, Shear stress	$E_c = c_0 S^{\nu}\left(\frac{Q}{W_c}\right)^{\mu}$
2, Under-capacity	$E_c = c_0 S^{\nu} Q^{\mu} - c_1 q$
2a, Under-capacity with channel width	$E_c = c_0 S^{\nu}\left(\frac{Q}{W_c}\right)^{\mu} - c_1\frac{q}{W_c}$
3, Sediment-limited	$E_c = \left[\left(S^{\nu}\left(\frac{Q}{W_c}\right)^{\mu}\right) - d_2\left(S^{\nu}\left(\frac{Q}{W_c}\right)^{\mu}\right)^2\right]\left(c_{1q} - c_{2q^2}\right)$
4, Threshold shear-stress	$E_c = c_0\left(\frac{SQ}{W_c} - b_0\right)^{\nu}$
5, Transport-limited	$E_c = c_0 S^{\nu}\left(\frac{Q}{W_c}\right)^{\mu}$
6, Sediment carrying and capacity sediment tools	$E_c = (c_0 S^{\nu}\left(\frac{Q}{W_c}\right)^{\mu} - c_1 q)(1 + c_2 q)$

[39] The expected values for ν and μ are debatable. *Willgoose et al.* [1991] use a total load equation, which gives $\nu = 2$ and $\mu = 1$. In contrast, a bed load-transport relation predicts $\nu = 1$, but provides no strong prediction for μ because of uncertainties related to downstream fining. We expect that μ in this case should be close to zero, but grain size may influence the sensitivity of incision to discharge. Given this lack of consensus, we allow a large range for values of ν, between 1 and 2, and μ, between 0 and 1.

3.6. Model 6: Shear Stress Incision With Sediment Carrying Capacity and Sediment Tools

[40] This model is an extension of model 2a in that increasing sediment discharge creates more tools for bedrock incision but transport of the sediment decreases the basal shear stress available for incision. The formulation used here is a simplified version of that suggested by *Slingerland et al.* [1997, 1998] in that the carrying capacity is assumed to be linear in slope and discharge. It has the same form as that of model 2a (equation (14)), save for the introduction of the positive constant c_2 that linearly links sediment discharge q to the rate of incision,

$$E_c = \left(c_0 S^{\nu}\left(\frac{Q}{W_c}\right)^{\mu} - c_1 q\right)(1 + c_2 q). \tag{21}$$

As formulated here, this model is an extension of model 2a and thus has the same expected values of μ and ν.

4. Model Testing

4.1. Statistical Methods

[41] Least squares analysis is used to test which of the competing channel incision models best accounts for the pattern of long-term incision rates for the Clearwater River. With each model, we find values for the free parameters (μ, ν, $c0$, $c1$, $c2$, and $b0$, as recast in Table 2) that allow the model to best fit the data. With this information, we can apply three tests:

[42] 1. Do the best fit models have physically plausible values? As noted above, we focus specifically on best fit estimates and uncertainties for the parameters ν and μ. At a minimum, we require that estimates of ν and μ should be greater than zero. We also consider how close the estimates come to the predictions from the literature, as outlined above.

[43] 2. Does a candidate best fit model fit the data well? A good fit will have residuals that are consistent with the predicted errors associated with the observed values for the model variables.

[44] 3. Are the residuals randomly distributed as a function of location along the river? The opposite case, where residuals show a correlated behavior, indicates a poor fit. Many of the solutions discussed below show correlated residuals. An example might be that the residuals are all positive along the lower reach of the river, and all negative along the upper reach.

[45] To summarize, we will reject a model if it fails to produce physically plausible parameters, or if its residuals are anomalously large or show systematic correlations along the length of the river.

[46] Our Clearwater data set (Table 1) is made up of measurements at $i = 1$ to N locations along the river, where $N = 57$. The model functions have up to five measured variables: long-term valley incision rate $E_{v,i}$, channel gradient S_i, mean annual water discharge Q_i, channel width $W_{c,i}$, and long-term sediment discharge q_i. We anticipate significant random errors for all of these measured variables. Furthermore, we expect that the random errors associated with the measured variables in this problem are roughly proportional to the magnitude of the variable (this result is commonly observed in ratioed data, such as the rate and slope data used here; see *Aitchison* [1986] for details). The implication is that the relative standard deviation for each of the variables in the data set is approximately constant.

[47] For situations like this, it is common practice to recast the model in a log-transformed form [*Aitchison*, 1986]. In our case, we define a generic least squares model

$$r_i = ln\left[\frac{f(S_i, Q_i, W_{c,i}, q_i)}{E_{v,i}}\right] + \sum[\epsilon_{ij}], \tag{22}$$

where r_i is the dependent variable. Random errors associated with measurements of $E_{v,i}$, S_i, Q_i, $W_{c,i}$, and q_i are represented by ϵ_{ij}, where $j = 1$ to 5 for the five variables. The ϵ values for the jth variable are considered to have a mean of zero and a standard deviation of α_j, indicating that there are five α values to represent the variation associated with the five variables.

[48] If an incision model is appropriate and the errors in the variables are random and uncorrelated, then r_i will have an expected value $E[r_i] = 0$. Thus r_i represents the residuals for the model fit.

[49] To explain the log transform, consider the fact that all of the incision models are based on the product of the observed variables. Furthermore, we have argued that the variables have approximately constant relative standard deviations. The log transform allows us to represent this situation using an α for each variable. Consider $E_{v,i}$ as an example. With the log transform, the errors for this variable are represented by $\ln[E_{v,i}] + (\epsilon_i)_E$, which means that the standard deviation of $\ln[E_{v,i}]$ is α_{E_v}. Consider that when α_{E_v} is small ($<\sim 0.07$), then $\ln[E_v] \pm \alpha_{E_v} \sim \ln[(1 \pm \alpha_{E_v})E_v]$. Thus α_{E_v} is approximately equal to the relative standard deviation of E_v. The same can be said of for each α, except for the fact that the errors for the other variables are multiplied by the parameters and coefficients in the best fit equation.

[50] It is important to emphasize that our analysis is similar to a conventional Least squares fit with $\ln[E_v]$ set as the dependent variable. One of the advantages of a log-transformed least squares function is that the errors associated with the observed variables end up being lumped together, so that they can be treated collectively as errors in the dependent variable r_i. This point can be illustrated by using the approximate formula for error propagation

$$\sigma_r^2 \sim \sum \alpha_j^2 \tag{23}$$

which shows that σ_r, the expected standard deviation of r, is constant and independent of the actual value of r_i (i.e., the variance of the residuals has been standardized to a common range).

[51] We do not know exactly what the α values are, but we expect that for individual variables, the relative standard deviations are on the order of 10 to 20%. In general, the best fit values for the parameters μ and ν have absolute values less than 1. Thus equation (23) indicates that σ_r should be no greater than 0.22 to 0.45, depending on how many variables are used in the fit equation and the estimated values for the parameters μ and ν. Note that this estimate only accounts for random errors, which is appropriate given that the least squares analysis is only able to resolve random errors. Any systematic errors are thought to be much smaller than 10%, but such errors would end up embedded in our estimate of the best fit parameters, and not in the residuals.

[52] The fit of a model to the data is defined by the chi-square statistic

$$\chi^2 = \sum\left(\frac{r_i}{\sigma_r}\right)^2. \tag{24}$$

A best fit model is determined by searching for a set of parameters that minimize χ^2 relative to the observed data. σ_r is an unknown constant, so in reality we end up minimizing Σr_i^2. An important advantage of our model function (equation 22) is that it has a linear form relative to the log-transformed parameters. Thus we can be assured that there is one and only one $\chi^2_{\min}$ solution. If the model is correct, then the expectation is that $\chi^2_{\min} \simeq (N - p)$, which is the degrees of freedom for the model fit with p = number of fit parameters in the model function. Thus σ_r can be estimated for a given best fit model using

$$\sigma_r^2 = \frac{\sum r_i^2}{(N - p)}. \tag{25}$$

The χ^2 statistic can also be used to determine confidence intervals for the estimated parameters [*Press et al.*, 1992, pp. 688–690]. We focus here on defining a joint confidence region for estimates of the μ and ν parameters. The objective is to determine if the 95% confidence region for the best fit solution includes physically plausible values for μ and ν. The method involves calculating $\chi^2_{\min}$ as a function of various values of fixed μ and ν. Of course, $\chi^2_{\min}(\mu, \nu)$ will increase from its global minimized value at the best fit solution for μ and ν, to higher values as we select less optimal values for μ and ν. Note that the other parameters of the model are allowed to take on optimal values for each μ, ν pair. Thus the resulting plot of $\chi^2_{\min}(\mu, \nu)$ represents a projection of χ^2_{min} in the full parameter space down on to the μ, ν plane. Confidence regions are defined by the relative value of χ^2 in the μ, ν plane as given by

$$\Delta\chi^2(\mu, \nu) = \chi^2_{\min}(\mu, \nu) - \chi^2_{\min}(\mu_{\text{best}}, \nu_{\text{best}}). \tag{26}$$

The 95% confidence region for two parameters is defined by the region where $\Delta\chi^2 \leq 6.17$ [*Press et al.*, 1992, p. 617].

[53] We use the Durbin-Watson method to test for serial correlations in residuals [*Draper and Smith*, 1998, pp. 181–182]. First, r_i is sorted so that the indice i indicates the residuals relative to their location upstream along the valley profile. The statistic for the test is given by

$$d = \frac{\sum_{i=2}^{N} \left[(r_i - r_{i-1})^2 \right]}{\sum_{i=1}^{N} \left[r_i^2 \right]}, \tag{27}$$

and has an expected value of $d = 2$ for no serial correlation in the residuals. We test for cases where there is a positive serial correlation, indicated by $d < 2$. Critical values depend on the number of residuals N, and also on the number of fit parameters, which ranges from 3 to 5 for the models considered here. Critical values of d are given as a range (d_u and d_l). We use the smaller d of this range to avoid false rejections of model solutions. Values for $d < 1.48$ to 1.41 (for models with 3 to 5 parameters, respectively) are considered evidence of significant positive serial correlation [*Draper and Smith*, 1998]. These values are given at the 5% significance level, so we are accepting that 1 out of 20 times, the failure of the test will be false.

[54] In our analysis below, we found that the Durbin-Watson test was strongly influenced by the last measurement at valley km 44. Almost all best fit solutions failed the test when this residual was included. This point may be an outlier, given that its incision rate is much lower than nearby measurements. Even so, this measurement had little influence on estimates of the parameters and their uncertainties. Thus we choose to retain the datum in our analysis, but to ignore it when calculating the Durbin-Watson statistic. This makes our criterion for rejection due to correlation even more conservative.

[55] These procedures provide the tools for implementing our three tests. The 95% confidence region allows us to test if the model and data predict physically plausible values for μ and ν. Estimates for σ_r allow us to judge the quality of the fit. Our estimate of errors suggests that a good model should have σ_r less than $\sim$0.4. Finally, randomly distributed residuals would require that d passes at the 5% significance level.

4.2. Model Comparison

[56] In this section, we judge the best fit estimates for each of the models. The results are illustrated in Figures 10, 11, 12, 13, 14, and 15, which show plots of σ_r and 95% and 99% confidence regions for the estimates of ν and μ (Table 2). Figures 10–15 also show the expected range for ν and μ as discussed for each model above. The residuals of the six models at their best fit solutions are shown in Figure 16. The best fit solutions shown in these figures have been calculated assuming the case of "hard incision," where channel incision is assumed to be fully responsible for the rate of valley incision. To do this, equation (2) was used to convert the observed valley incision rates to corresponding channel incision rates, which were then fit relative to the model equations (Table 2). The estimated ν and μ are thus representative of this hard incision case, which we suspect is the more likely situation. We have not shown solutions for

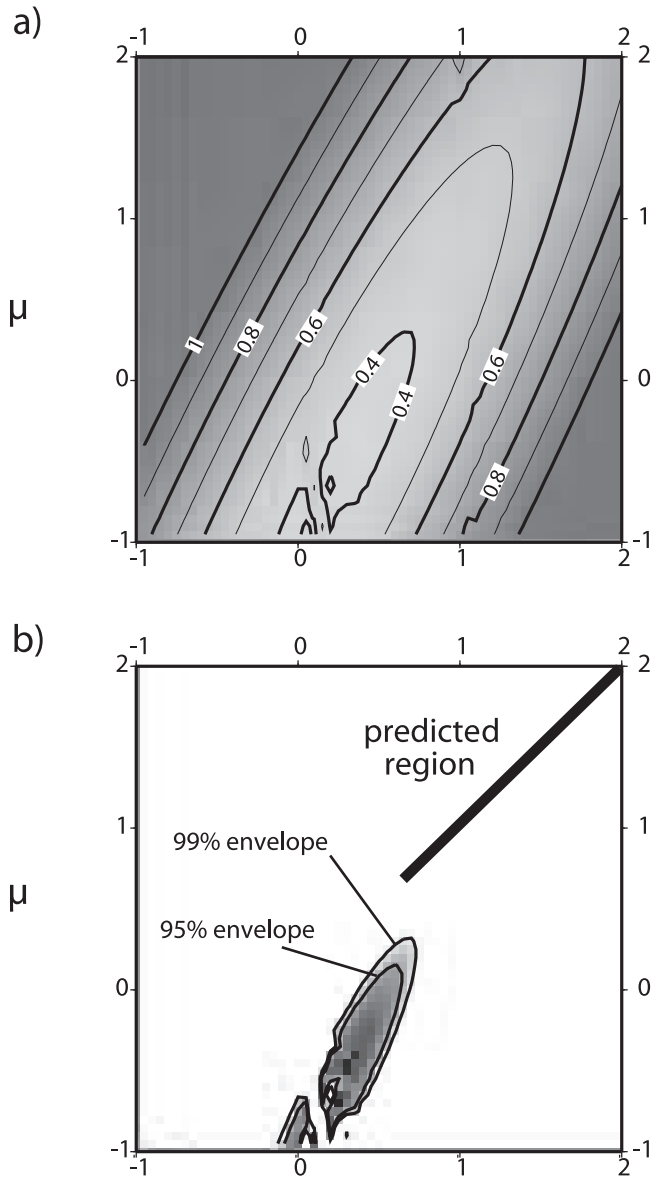

Figure 10. Results for model 1, shear stress incision. The diagonal line marks $\mu = \nu$ and is used in the discussion of model 4, the threshold shear stress model. (a) Contour map for estimates of σ_r as a function of μ and ν. The intervals are equal to 0.1 where $\sigma_r \leq 1$ and 5 where $\sigma_r > 1$. (b) Contour map showing 95% and 99% confidence regions for best fit estimates of μ and ν. The black line shows the range of μ and ν predicted for model. The best fit point is $\mu = -0.40$, $\nu = 0.35$ (with $c_0 = 7.0$).

"easy incision," where $E_\nu = E_c$, but in all cases these solutions are the same as those for hard incision, except that they are offset downward parallel to the μ axis by 0.72. This offset is based on the following scaling relationship, $E_\nu \propto E_c (Q/W_c)^f$, derived from (5) and (8). Form the Clearwater, $f = 0.38/(b - 1) = 0.72$. This relationship shows that the difference between E_ν and E_c can be entirely represented by the normalized discharge raised to a power. As such, the difference between easy and hard incision only affects the predictions for μ and by a specific offset equal to f.

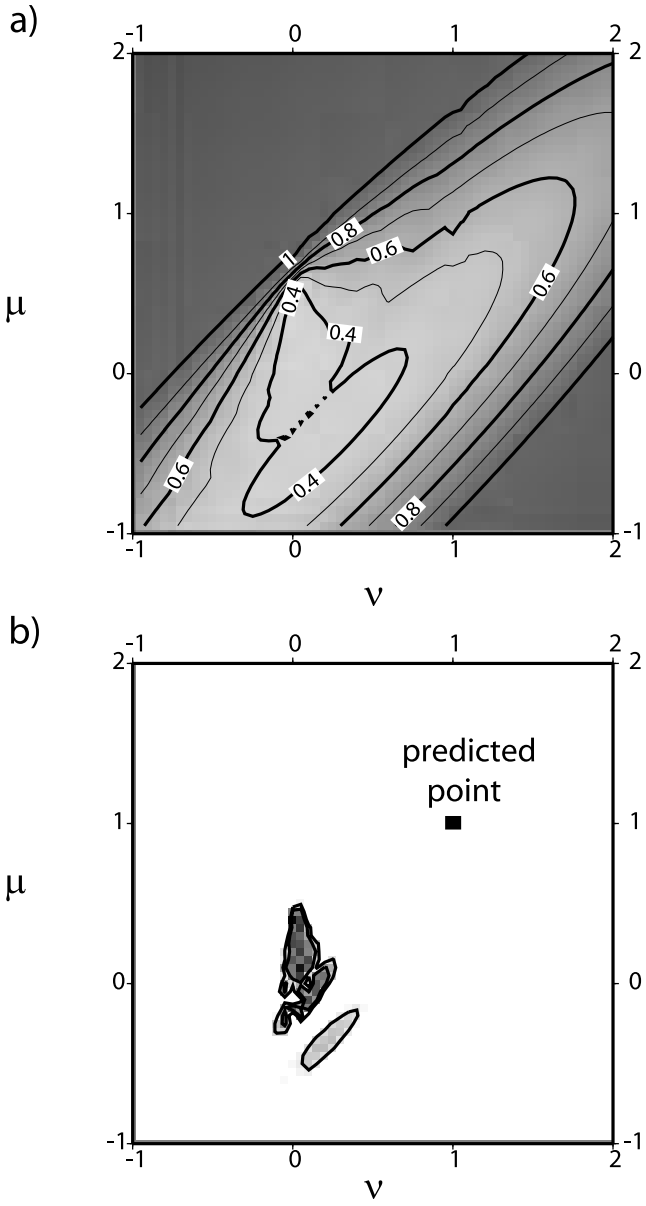

Figure 11. Results for model 2, under-capacity incision. Contour maps show (a) σ_r estimates as a function of μ and ν, and (b) 95% and 99% confidence estimates of μ and ν (see Figure 10 for details). The best fit point is $\mu = 0.4$, $\nu = 0.0$ (with $c_0 = 3.8$, and $c_1 = -9 \times 10^{-5}$).

[57] Three tests are applied to the models (in accordance with section 4.1). A general conclusion is that none of the incision models provide a good fit to the Clearwater data. The problem is that the best fit solutions always give unacceptably low estimates for μ or ν. They otherwise have reasonable residuals, both in size ($\sigma_r < 0.4$) and random distribution. We have also tried fitting the models to parts of the river, with the idea that the upper or lower reaches of the river might be influenced by different fluvial processes. Even in these cases, the best fit solutions indicate very small values for μ and ν. We have explored solutions where μ and ν are forced to take on values within the predicted ranges, but those solutions always have strongly correlated residuals. We now examine this conclusion on a case-by-case basis.

4.2.1. Model 1: Shear Stress Incision

[58] Using the Clearwater data, the best fit solution for the model gives $\nu = 0.35$ and $\mu = -0.40$, as defined by the minimum σ_r in Figure 10a. The best fit solution has a tolerable σ_r value (i.e., <0.4), but the solution seems implausible in that the estimated μ is negative. The 95% confidence region includes positive estimates for both ν and μ, but the residuals become more highly correlated away from the best fit solution. For instance, the 95% confidence region permits more plausible estimates of $\mu = 0.1$ and $\nu = 0.7$, but these extreme values cause the model

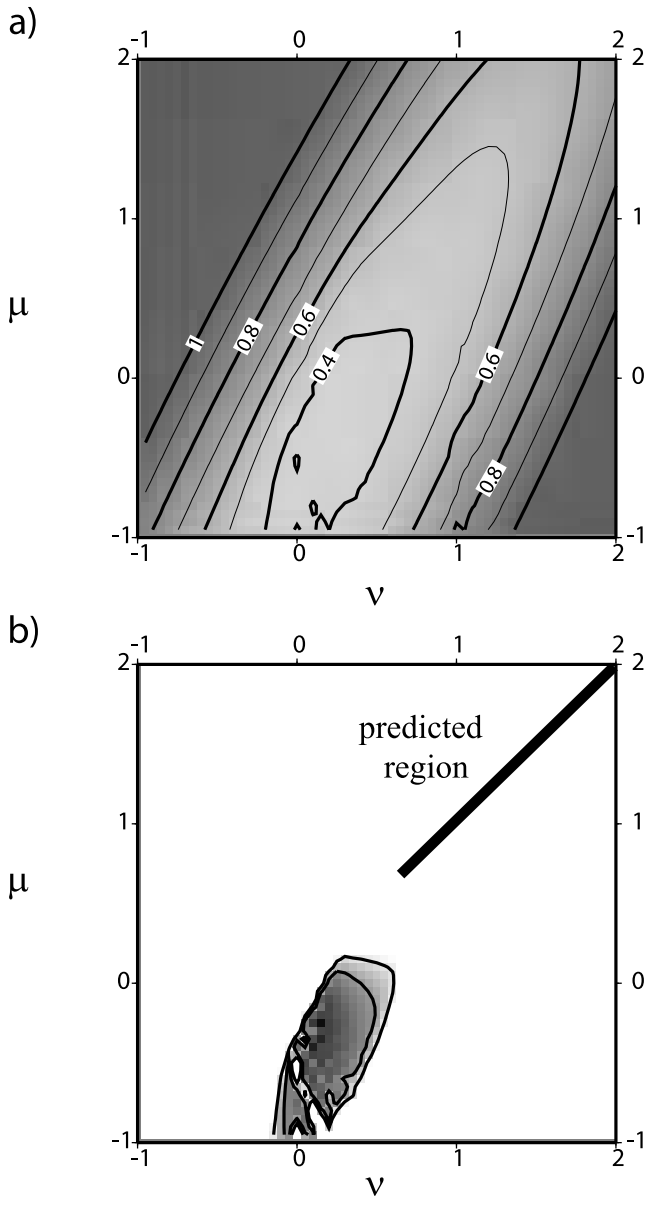

Figure 12. Results for model 2a, under-capacity incision with channel width correction. Contour maps show (a) σ_r estimates as a function of μ and ν, and (b) 95% and 99% confidence estimates of μ and ν (see Figure 10 for details). The best fit point is $\mu = -0.25$, $\nu = 0.15$ (with $c_0 = 5.0$, and $c_1 = -4.6 \times 10^{-4}$).

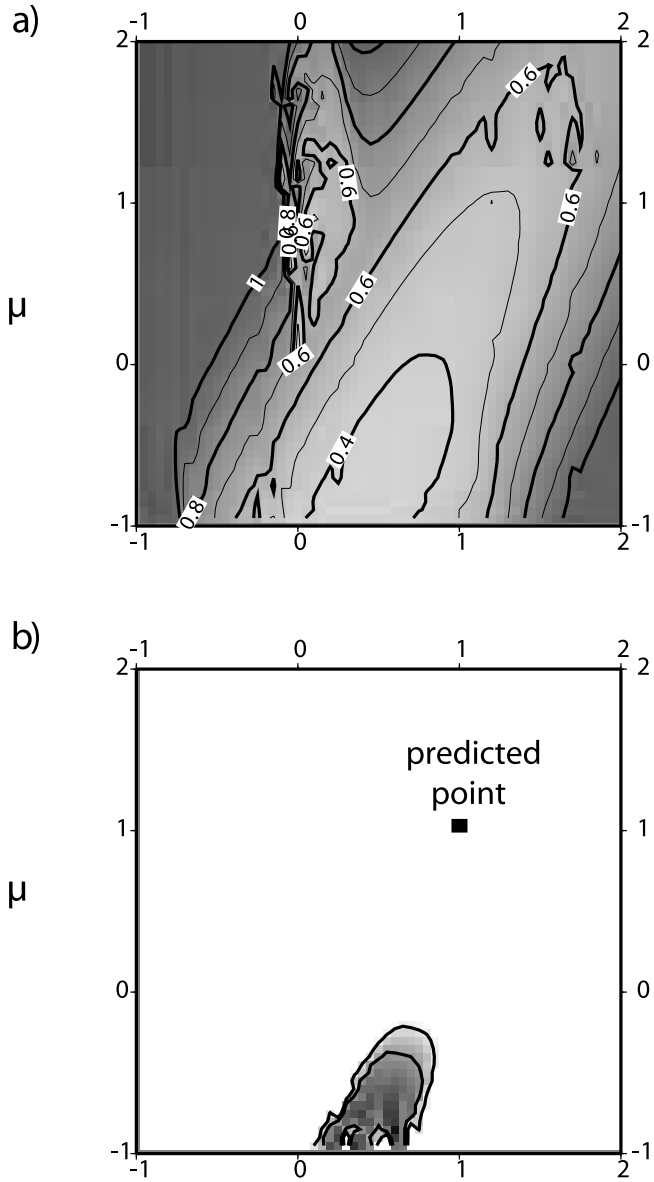

Figure 13. Results for model 3, sediment-limited incision. Contour maps show (a) σ_r estimates as a function of μ and ν, and (b) 95% and 99% confidence estimates of μ and ν (see Figure 10 for details). The best fit point is $\mu = -0.95$, $\nu = 0.35$ (with $c_1 = d_1 = 0.0$, and $c_2 = 1.5 \times 10^{-3}$).

to systematically underestimate incision rates in the upper part of the drainage (d = 0.34). In summary, the shear stress incision model is incompatible with the Clearwater data.

4.2.2. Model 2: Under-Capacity Incision

[59] The best fit estimates (Figure 11) for the under-capacity model, $\nu = 0.0$ and $\mu = 0.4$, are physically implausible in that the estimated ν is zero. The 95% confidence interval permits values ν of up to 0.2, but even this value is too small to be plausible. Furthermore, estimates other than the best fit values tend to give strongly correlated residuals. Recall that model 2 has an extra term that accounts for varying sediment discharge. This might lead one to expect that model 2 would out perform model 1. The opposite is the case: model 2 does a poorer job than model 1 in fitting the Clearwater data.

[60] Model 2a, which is normalized to account for the width of the channel, is also deficient. The best fit estimates of $\nu = 0.15$ and $\mu = -0.25$ (Figure 12) give a tolerable σ_r value (i.e., <0.4), but the negative μ renders the solution implausible. The 95% confidence region includes positive estimates for both ν and μ of up to 0.5 and 0.1, respectively, but at these ν and μ values the residuals are serially correlated, with a Durbin-Watson statistic of 1.19.

4.2.3. Model 3: Sediment-Limited Incision

[61] The best fit solution for this model gives $\nu = 0.35$ and $\mu = -0.95$, with an acceptable σ_r of less than 0.4 (Figure 13a). All μ values in the 95% confidence region are negative and are thus physically implausible.

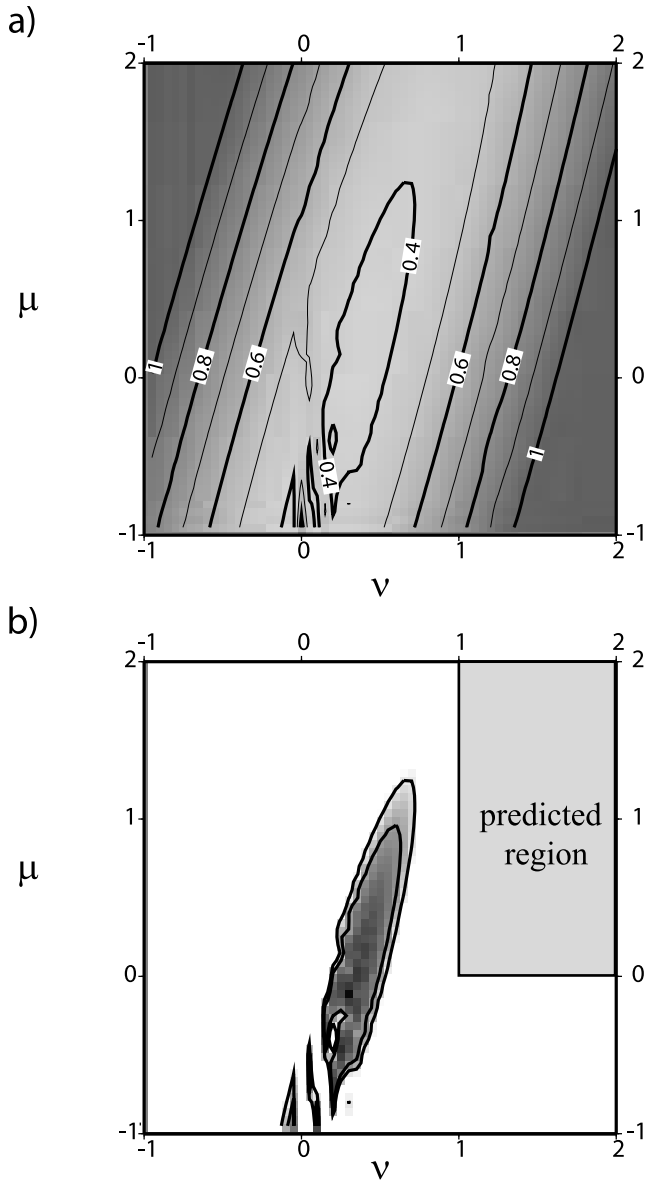

Figure 14. Results for model 5, transport-limited incision. Contour maps show (a) σ_r estimates as a function of μ and ν, and (b) 95% and 99% confidence estimates of μ and ν (see Figure 10 for details). The best fit point is $\mu = -0.10$, $\nu = 0.30$ (with $c_0 = 5.0$).

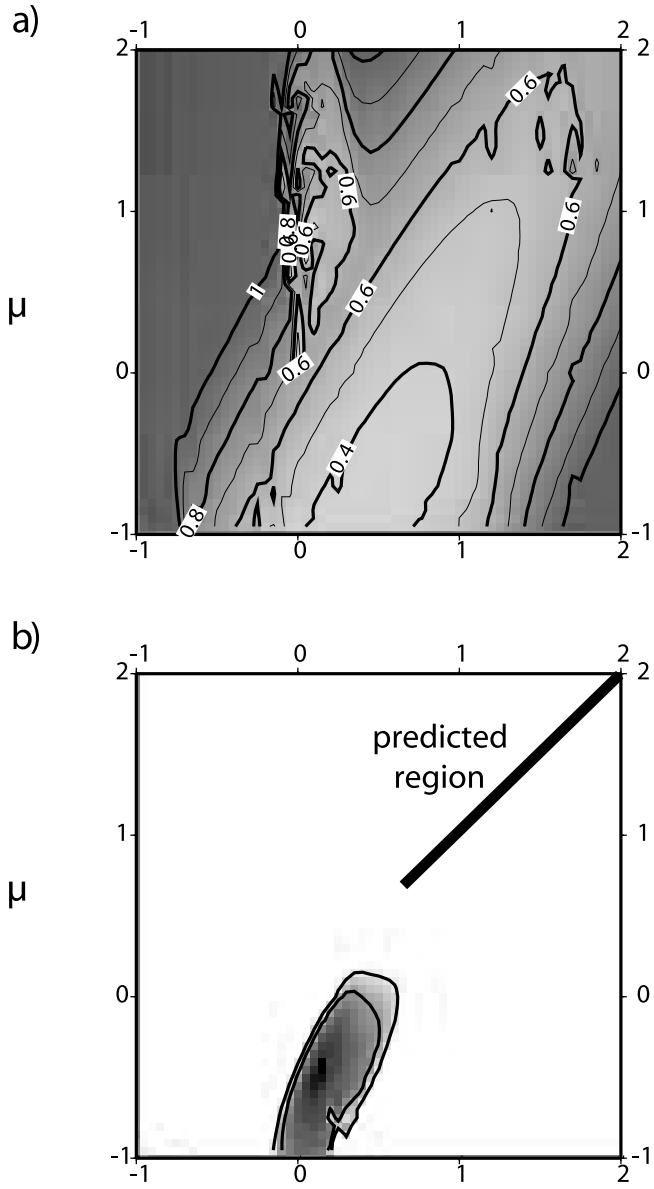

Figure 15. Results for model 6, sediment carrying capacity and sediment tools incision. Contour maps show (a) σ_r estimates as a function of μ and ν, and (b) 95% and 99% confidence estimates of μ and ν (see Figure 10 for details). The best fit point is $\mu = -0.40$, $\nu = 0.15$ (with $c_0 = 3.25$, $c_1 = -3.0 \times 10^{-4}$, and $c_2 = 6.0 \times 10^{-6}$).

No solution to the data is compatible with the Clearwater data.

4.2.4. Model 4: Threshold Shear Stress Incision

[62] The best fit solution for the model gives $\nu = 0.55$ (with $c_0 = 68.9$, $b_0 = 0.00050$). Note that the estimated b_0 value is very small, which means that there is little difference between this model and model 1, other than the fact that model 4 specifies that $\nu = \mu$. As a result, the best fit solution is already illustrated in Figure 10, with the restriction that the solution must lie along the diagonal lines marking $\mu = \nu$. The σ_r value is 0.45, which is unacceptably large. In addition, the residuals are serially correlated for this solution, with a Durbin-Watson value of 1.02. Other values of ν give even worse fits, with larger σ_r and more strongly correlated residuals.

[63] The b_0 parameter in model 4 is meant to account for a threshold shear stress nedded to initiate incision. The threshold parameter in model 4 makes the incision rate sensitive to the distribution of discharges in the river [*Tucker and Slingerland*, 1997]. For our analysis, we have represented the discharge at each position along the river by a single value, the mean annual discharge. This compromise is common in studies of mountain rivers where long discharge records are typically not available. Nonetheless, we can infer how model 4 might perform if detailed discharge information were available for the Clearwater. For physically plausible values of ν (i.e., $\nu > 0$), an increase in the b_0 threshold would lead to greater incision downstream where peak discharges would be larger. Our solution for model 4, which ignores the distribution of discharge, already overpredicts incision rates along the lower reach of the river. This shows up as a systematic misfit along the lower reach (Figure 16). Thus addition of discharge distributions to the model would not improve the fit to the data. From this, we conclude that threshold effect is probably not an important factor for long-term incision of the Clearwater.

4.2.5. Model 5: Transport-Limited Stream Power

[64] The best fit solution for this model gives $\nu = 0.30$ and $\mu = -0.10$, with an acceptable σ_r of less than 0.4 (Figure 14a). This solution is implausible in that the estimated μ is negative. The 95% confidence region includes positive estimates for both ν and μ, but the residuals become more highly correlated away from the best fit solution. For instance, the 95% confidence region permits high estimates of $\mu = 0.95$ and $\nu = 0.6$, but the Durbin-Watson statistic of 1.16 at this point indicates that the residuals are strongly serially correlated for this μ, ν estimate.

4.2.6. Model 6: Shear Stress Incision With Sediment Carrying Capacity and Sediment Tools

[65] The best fit solution for this model gives $\nu = 0.15$ and $\mu = -0.40$, with an acceptable σ_r of less than 0.4 (Figure 15a). This solution is implausible in that the estimated μ is negative. The model has a result similar to those of models 1 and 2, and fails in the same way as well. Although the 95% confidence region includes positive estimates for both ν and μ, but the residuals become more highly correlated away from the best fit solution. This model is incompatible with the Clearwater data.

5. Valley Slope Versus Channel Slope

[66] Our analysis suggests that none of the available incision models provides a good fit to the Clearwater data. Discharge increases downstream, so some other factor is needed to allow the river to compensate for the observed downstream decrease in the long-term incision rate. Sediment discharge increases downstream, but models that incorporate q (models 2, 3, and 6) indicate that this variable does not provide an obvious solution. Channel slope decreases downstream, but, as illustrated by the fit using model 1, the downstream change in slope is not large enough to give physically plausible parameters, where μ and ν are both greater than zero.

[67] One problem with our analysis is that we have mixed long-term features of the river, such as incision rates and

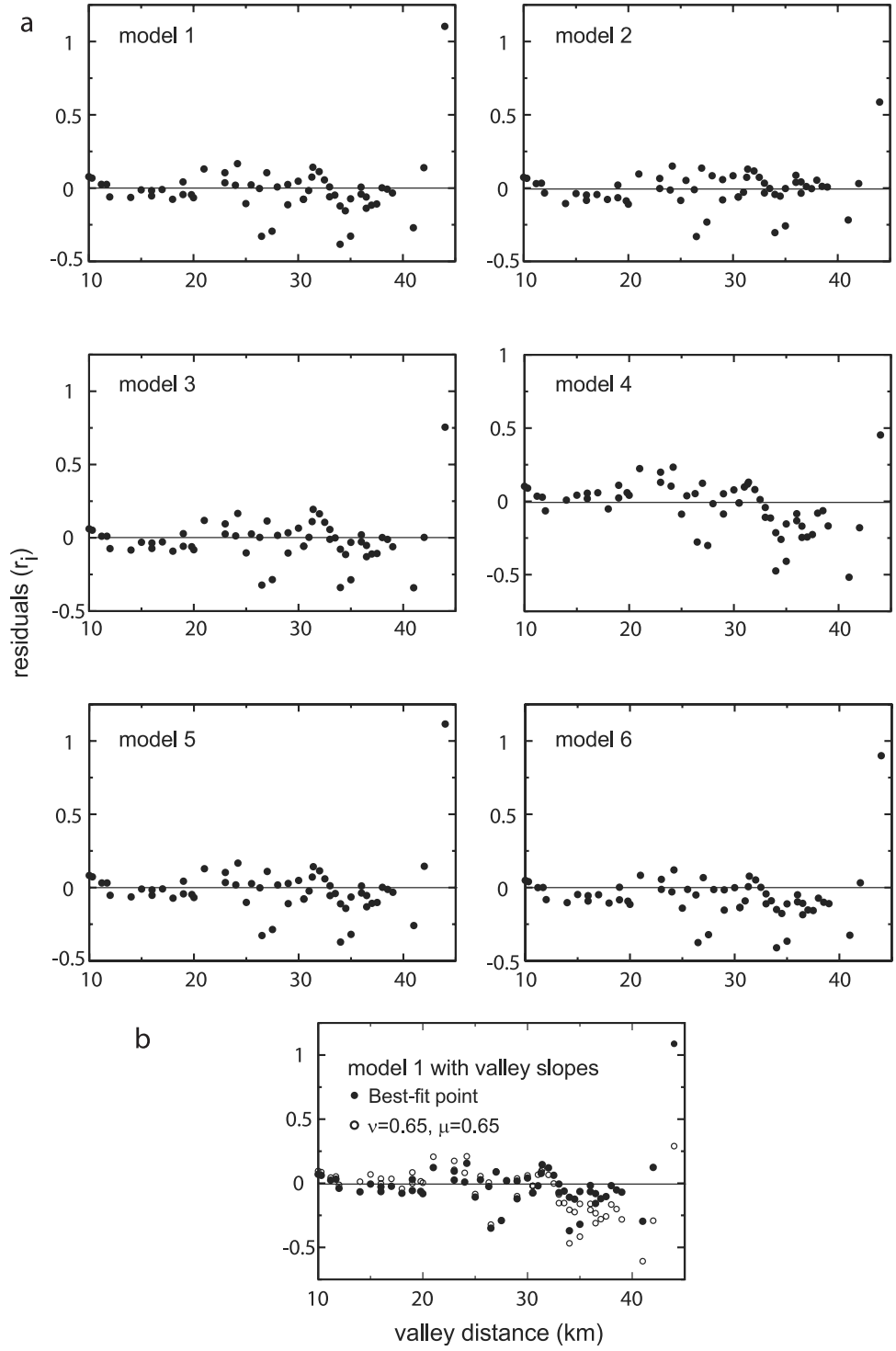

Figure 16. (a) Pattern of residuals for the 6 models at their best fit points as a function of valley distance, and (b) the pattern of residuals of model 1 when valley slopes are used in place of channel slopes.

sediment discharge, with short-term features, such as the modern water discharge, channel width, and channel slope. An important question is if the modern data are in fact representative of the long-term character of the river. Water and sediment discharges are expected to vary with climate, but both of these variables would still increase steadily downstream, in a manner similar to modern water and sediment discharges.

[68] In contrast, channel slope can change rapidly and independently at any point along the river. Our channel slope measurements show considerable variance at short wavelengths along the river. Some of this variation is mirrored by short-wavelength variations in incision rate. For instance, *Pazzaglia and Brandon* [2001] argue that the pattern of channel sinuosity between km 20 and 28 of the river indicates a slowly growing anticline there. The straths

show a corresponding upwarping across this region, consistent with an actively rising structure. However, there is little further evidence that short-wavelength variations in channel slope are everywhere matched by corresponding variations in rock uplift rate.

[69] In addition, it can be stated that neither the upwarping, nor the poor fit between the data and the models, is a consequence of different processes operating in the bedrock-dominated upper reach versus the alluvial-dominated lower reach. If the data are split into two sections (one below the major confluence of the Snahapish River (which joins the Clearwater River at about the 25 km mark) and one above) the individual data sets produce best fit μ or ν values that are very similar to those produced by the full data set.

[70] An alternative explanation is that variance in channel slope is due to small migrating knickpoints. Short-wavelength features in the channel should propagate relatively quickly along the length of the channel [*Whipple and Tucker*, 1999]. These ephemeral features would appear as noise in our analysis. We have attempted to reduce the influence of these features by using a 3-km-long moving regression window to smooth out local features in the channel. This level of smoothing is used by others studying bedrock incision (K. Whipple, personal communication, 2001), so our analysis is on a similar footing. The problem, however, is that the selected level of smoothing is ad hoc. There is no assurance that we have fully removed the influence of short-term features from the channel data.

[71] In fact, we are left to wonder if one of the incision models might show a better fit if the slope data were more heavily smoothed. To consider this question, we repeat our analysis for model 1 using the slope of the Clearwater valley as a proxy for the long-term slope of the river. As noted above, the straths record long-term incision of the river valley. The inference is that the valley slope should be a more stable feature of the landscape, and thus should be more closely linked to the timescale represented by the straths. Valley slope is steeper than the channel slope because of the sinuosity of the channel. The valley slope is smoother as well because of the longer length scale used to make this measurement.

[72] Our analysis of model 1 using valley slopes is shown in Figure 17. The best fit solution, with $\mu = -0.35$ and $\nu = 0.45$, is similar to that for the original analysis of model 1 using channel slopes. The negative value for μ makes the best fit solution physically implausible. An important difference of the fit for the valley slope model is that the 95 percent uncertainty region for μ and ν is much larger. This near overlap does not indicate that any values within the confidence region provide a successful fit to the data. In fact, the residuals become strongly correlated away from the best fit solution. For example, a predicted solution with $\mu = \nu = 0.65$ has d = 0.83, which indicates a strong failure of the Durbin-Watson test. The predicted region is thus rejected as a solution because of strongly correlated residuals in that part of the parameter space.

[73] All of the models show the same result when using more highly smoothed slope data. The smoothed slope data will tend to increase the correlation of μ and ν, and thus will extend the long axis of the elliptical uncertainty region for μ and ν in the direction of their common correlation. Thus an important conclusion is that regression analysis of incision models is best conducted for rivers that have a low correlation between slope and discharge. This condition is provided by using rivers that have spatially varying rock uplift rates along their course. A river crossing an actively growing anticline would be a good example.

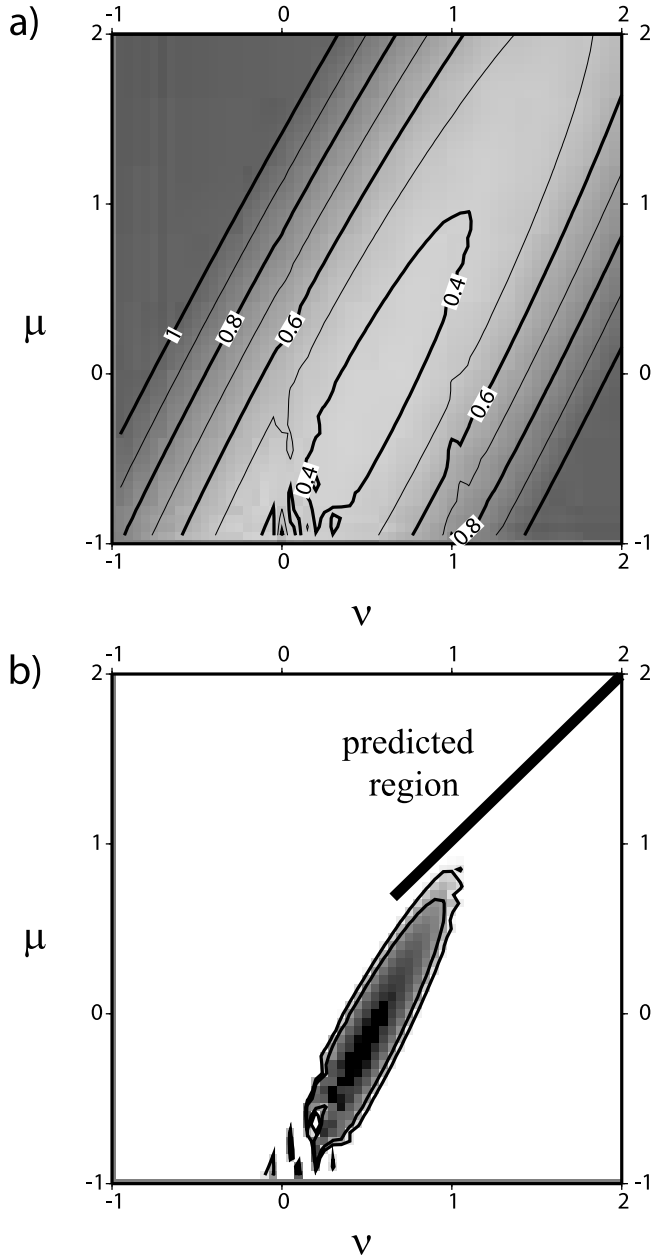

Figure 17. Results for model 1, shear stress incision, when valley slope replaces channel slope. Contour maps show (a) σ_r estimates as a function of μ and ν, and (b) 95% and 99% confidence estimates of μ and ν (see Figure 10 for details). The best fit point is $\mu = -0.45$, $\nu = 0.35$ (with $c_0 = 6.0$).

[74] A second conclusion, however, is that even when the uncertainty region is large, a model can fail due to strong serial correlation in its residual. On this basis, we conclude that none of the models, as presently implemented, is

successful in fit the data. Either the best fit parameters are physically implausible (i.e., μ and ν less than zero) or the predicted values for the parameters have strongly correlated residuals.

6. Discussion

[75] Our analysis prompts us to question the applicability of available bedrock incision models for the Clearwater River. In particular, the popular shear stress incision model seems incompatible with our incision data for the Clearwater. Others [*Siedel and Dietrich*, 1992; *Stock and Montgomery*, 1999; *Wohl*, 2000, pp. 54–55] have encountered difficulties when comparing the stream power model with real incision data. The problems are usually attributed to changes in base level, migrating knickpoints, or nonuniform lithology along the channel. In most of these studies, rock uplift velocities were unknown and were assumed to be uniform along the analyzed stretch of the river. All of these factors can be accounted for in our Clearwater study. Uplift velocities are well constrained and known to be steady over the timescale represented by the incision data. Lithology is fairly homogeneous, base level has been relatively steady, and major knickpoints are not present.

[76] Failure of the shear stress model motivated the analysis in this paper of a variety of incision models. We were surprised to find that none of the available incision models provided an adequate fit. Nonetheless, we agree that the physical processes represented by the models, such as abrasion, bed coverage, tool impact, etc., should be useful in predicting the rate of bedrock incision. If this intuition is correct, then something must be missing from the way the models are implemented. If we use the Clearwater as a guide, then there must be a physically plausible explanation as to how increasing incision rate correlates with decreasing normalized discharge (Q/Wc).

[77] We propose that assumptions about discharge may be the critical factor. Discharge in a river is neither steady nor always confined to the channel [*Tucker and Bras*, 2000]. The power exponent for discharge, defined by μ in this paper, determines the influence of stochastic flow variability on the incision process. When μ is less than one, most of the incision will be done during the smaller steady discharges, but when μ is greater than one, incision will occur mainly during the largest discharges. Thus we can define an effective discharge that corresponds to the discharge that does most of the incision [*Knighton*, 1984, pp. 94–96; *Wohl*, 2000, p. 111]. However, there is another factor, in that the size of the channel determines the bankfull discharge, which is the maximum discharge that the river can pass without over spilling its banks [*Knighton*, 1984; *Wohl*, 2000]. When the discharge goes beyond bankfull, the excess flow is no longer confined, and will spread out laterally and slow down. As a result, the overbank flow contributes nothing to incision of the channel. Thus incision models should ignore discharge greater than bankfull.

[78] The problem with mountain rivers is that the channel configuration varies greatly along the length of the river. Deeply incised gorges are common in the upper reaches. Such gorges probably rarely, if ever, see a bankfull discharge. Thus all parts of the discharge distribution will contribute to channel incision. In contrast, the lower reaches commonly have broader river valleys, which will frequently have flows that exceed bankfull.

[79] We have already noted that the threshold shear stress model can have a strong sensitivity to the distribution in discharge. Our discussion here indicates that all incision models are sensitive to the discharge distribution because of natural variations in the channel size along the course of the river. In other words, a big storm might cause a lot of incision in the upper reach of a mountain river, but the lower reach will be less affected because the flow will exceed bankfull.

[80] In our analysis above, we have normalized the mean discharge by the width of the channel. Thus our suggestion here is that upper reach of the Clearwater has seen more frequent deeper and faster flows relative to the lower reach. In other words, our prediction is that the normalized effective discharge decreases downstream. Normalized effective discharge may also have an important influence on strath formation. Incision may operate rapidly when the river is confined to a narrow gorge, but as the river is able to widen the adjacent valley floor (i.e., cut a strath), more of the largest discharges are passed as overbank flows. The rate of vertical incision should slow as a consequence.

[81] We have no direct evidence for that these ideas, but they highlight the simplifications implicit in many of the models that all of the flow in the river contributes equally to bedrock incision. This assumption is inherent in the proposal that incision rate should be proportional to $(Q/W_c)^{\mu}$, as specified here, or A^m, as invoked in the stream power model. We speculate that for the Clearwater, the bankfull discharge might account for why the lower reach of the river is able to adjust to a slower long-term uplift rate, while the upper reach is still able to keep pace with the faster uplift rate there.

7. Concluding Remarks

[82] Our study is the first to make detailed tests of a range of competing incision models using long-term incision rate data. The results are surprising, in that none of the models are able to account for the observations. Several conclusions are indicated:

[83] 1. Previous attempts to test incision models have sometimes assumed that rock uplift rates were uniform along the length of the river. The Clearwater River provides a clear example where this is not the case. We hope that future work will attempt to incorporate independent information about rock uplift rates. Horizontal shortening may also be important in some cases, as discussed by *Pazzaglia and Brandon* [2001].

[84] 2. We see little reason at this time to favor any specific model for bedrock incision. Further testing is needed on well characterized rivers before any firm conclusions can be made about the viability of specific models. As a result, we advise caution in using any of the available incision models for modeling or analysis of tectonic problems. Likewise, use of slope-area plots as an interpretational tool should be avoided, given that it relies on the assumption that incision along the course of the river can be described by a single stream power relationship and that rock uplift is uniform along the river.

[85] 3. There is clearly a problem in relating long-term incision rate determined from straths to the modern meas-

urements of discharge and channel form. Slope and width data are commonly smoothed, but there has been no study of whether smoothing is really needed, and how much smoothing should be applied. In fact, the short-wavelength variations in slope and width may contain some information about incision processes. Further consideration is needed to determine what measure of slope, either channel or valley slope, is best related to long-term incision rate.

[86] 4. Our study highlights the importance of finding rivers where rock uplift rates vary spatially along the length of the river and where the steadiness of that uplift can be assessed. Greater variability in uplift along the river would decrease the correlation between slope and area, and would allow better resolution of parameters using regression analysis. A good example of an ideal study area would be a river that crossed one or more short-wavelength anticlines.

[87] 5. For all the models considered, including those in which sediment discharge is included as a variable, both μ and ν tend to be lower than predicted. This has implications for the response time of the Clearwater drainage to tectonic and climatic changes. A low value for μ implies that large changes in discharge will cause relatively small changes in incision rate. In contrast, a low value for ν implies that changes in the rock uplift rate would require large changes in channel slope, and, by association, topographic relief. As a result, our analysis suggests that topography in the Olympics Mountains would respond relatively quickly to change in climate, but relatively slowly to changes in rock uplift rates.

References

Aitchison, J., *The Statistical Analysis of Compositional Data*, 416 pp., Chapman and Hall, New York, 1986.

Armstrong, A. C., Soils and slopes in a humid environment, *Catena*, *7*, 327–338, 1980.

Barbour, J. R., The utility of a stream power law for bedrock incision in the Olympic Mountains, WA, Senior thesis, 35 pp., Yale Univ., New Haven, 1998.

Batt, G. E., M. T. Brandon, and K. A. Farley, Tectonic synthesis of the Olympic Mountains segment of the Cascadia wedge, using two-dimensional thermal and kinematic modeling of thermochronological ages, *J. Geophys. Res.*, *106*, 26,731–26,746, 2001.

Beaumont, C., P. Fullsack, and J. Hamilton, Erosional control of active compressional orogens, in *Thrust Tectonics*, edited by K. R. McClay, pp. 1–18, Kluwer Acad., Norwell, Mass., 1992.

Begin, S. B., D. F. Meyer, and S. A. Schumm, Development of longitudinal profiles of alluvial channels in response to base-level lowering, *Earth Surf. Processes Landforms*, *6*, 49–68, 1981.

Brandon, M. T., M. K. Roden-Tice, and J. I. Garver, Late Cenozoic exhumation of the Cascadia accretionary wedge in the Olympic Mountains, northwest Washington State, *Geol. Soc. Am. Bull.*, *110*, 985–1009, 1998.

Bull, W. B., Threshold of critical power in streams, *Geol. Soc. Am. Bull.*, *90*, 453–464, 1979.

Bull, W. B., *Geomorphic Response to Climate Change*, 326 pp., Oxford Univ. Press, New York, 1991.

Chase, C. G., Fluvial landsculpting and the fractal dimension of topography, *Geomorphology*, *5*, 39–57, 1992.

Daly, C., R. P. Neilson, and D. L. Phillips, A statistical-topographic model for mapping climatological precipitation over mountainous terrain, *J. Appl. Meteorol.*, *33*, 140–158, 1994.

Daly, C., G. H. Taylor, W. P. Gibson, T. W. Parzybok, G. L. Johnson, and P. Pasteris, High-quality spatial climate data sets for the United States and beyond, *Trans. Am. Soc. Agric. Eng.*, *43*, 1957–1962, 2001.

Draper, N. R., and H. Smith, *Applied Regression Analysis*, 3rd ed., 706 pp., John Wiley, New York, 1998.

Dunne, T., and L. B. Leopold, *Water in Environmental Planning*, 818 pp., W. H. Freeman, New York, 1978.

Gilbert, G. K., Report on the geology of the Henry Mountains, Geogr. and Geol. Surv. of the Rocky Mt. Region, Govt. Print. Off., Washington, D. C., 1877.

Hancock, G. S., and R. S. Anderson, Numerical modeling of fluvial strath-terrace formation in response to oscillating climate, *Geol. Soc. Am. Bull.*, *114*, 1131–1142, 2002.

Hancock, G. S., R. S. Anderson, and K. X. Whipple, Beyond power: Bedrock incision and form, in *Rivers Over Rock: Fluvial Processes in Bedrock Channels*, *Geophys. Monogr. Ser.*, vol. 107, edited by K. J. Tinkler and E. E. Wohl, pp. 35–60, AGU, Washington, D. C., 1998.

Howard, A. D., Badland morphology and evolution: Interpretation using a simulation model, *Earth Surf. Processes Landforms*, *22*, 211–227, 1997.

Howard, A. D., and G. Kerby, Channel changes in badlands, *Geol. Soc. Am. Bull.*, *94*, 739–752, 1983.

Howard, A. D., W. E. Dietrich, and M. A. Seidl, Modeling fluvial erosion on regional to continental scales, *J. Geophys. Res.*, *99*, 13,971–13,986, 1994.

Knighton, D., *Fluvial Forms and Processes*, 218 pp., Edward Arnold, London, 1984.

Kooi, H., and C. Beaumont, Large-scale geomorphology: Classical concepts reconciled and integrated with contemporary ideas via a surface processes model, *J. Geophys. Res.*, *101*, 3361–3386, 1996.

Leopold, L. B., *A View of the River*, 298 pp., Harvard Univ. Press, Cambridge, Mass., 1994.

Leopold, L. B., and J. P. Miller, Ephemeral streams—Hydraulic factors and their relation to the drainage network, *U.S. Geol. Surv. Prof. Pap.*, *282A*, 1956.

Montgomery, D. R., T. B. Abbe, J. M. Buffington, N. P. Peterson, K. M. Schmidt, and J. D. Stock, Distribution of bedrock and alluvial channels in forested mountain drainage basins, *Nature*, *381*, 587–589, 1996.

Pazzaglia, F. J., and M. T. Brandon, A fluvial record of long-term steady-state uplift and erosion across the Cascadia Forearc High, western Washington State, *Am. J. Sci.*, *301*, 385–431, 2001.

Press, W. H., S. A. Teukolsky, W. T. Vetterling, and B. P. Flannery, *Numerical Recipes in FORTRAN*, 2nd ed., 963 pp., Cambridge Univ. Press, New York, 1992.

Seidl, M. A., and W. E. Dietrich, The problem of channel erosion into bedrock, *Catena Suppl.*, *23*, 101–124, 1992.

Sklar, L., and W. E. Dietrich, River longitudinal profiles and bedrock incision models: Stream power and the influence of sediment supply, in *Rivers Over Rock: Fluvial Processes in Bedrock Channels*, *Geophys. Monogr. Ser.*, vol. 107, pp. 237–260, AGU, Washington, D. C., 1998.

Sklar, L., and W. E. Dietrich, Sediment strength controls on river incision into bedrock, *Geology*, *29*, 1087–1090, 2001.

Slingerland, R., S. Willett, and H. L. Hennessey, A new fluvial bedrock erosion model based on the work-energy principle, *Eos Trans. AGU*, *78* (46), Fall Meet. Suppl., F299, 1997.

Slingerland, R., S. D. Willett, and N. Hovius, Slope-area scaling as a test of fluvial bedrock erosion laws, *Eos Trans. AGU*, *79*(45), Fall Meet. Suppl., F358, 1998.

Snyder, N. P., K. X. Whipple, G. E. Tucker, and D. J. Merrits, Landscape response to tectonic forcing: Digital elevation model analysis of stream profiles in the Mendocino triple junction region, northern California, *Geol. Soc. Am. Bull.*, *112*, 1250–1263, 2001.

Stock, J. D., and D. R. Montgomery, Geologic constraints on bedrock river incision using the stream power law, *J. Geophys. Res.*, *104*, 4983–4993, 1999.

Strahler, A. N., Quantitative geomorphology of drainage basins and channel networks, in *Handbook of Applied Hydrology*, pp. 4–39, McGraw-Hill, New York, 1964.

Tabor, R. W., and W. M. Cady, The structure of the Olympic Mountains, Washington—Analysis of a subduction zone, *U.S. Geol. Surv. Prof. Pap.*, *1033*, 38 pp., 1978.

Tinkler, K. J., and E. E. Wohl (Eds.), *Rivers Over Rock: Fluvial Processes in Bedrock Channels*, *Geophys. Monogr. Ser.*, vol. 107, 340 pp., AGU, Washington, D. C., 1998.

Tucker, G. E., and R. L. Bras, A stochastic approach to modeling the role of rainfall variability in drainage basin evolution, *Water Resour. Res.*, *36*, 1953–1965, 2000.

Tucker, G. E., and R. L. Slingerland, Erosional dynamics, flexural isostasy, and long-lived escarpments: A numerical modeling study, *J. Geophys. Res.*, *99*, 12,229–12,243, 1994.

Tucker, G. E., and R. L. Slingerland, Drainage basin response to climate change, *Water Resour. Res.*, *33*, 2031–2047, 1997.

Tucker, G. E., and K. X. Whipple, Topographic outcomes predicted by stream erosion models: Sensitivity analysis and intermodel comparison, *J. Geophys. Res.*, *107*(B9), 2179, doi:10.1029/2001JB000162, 2002.

U.S. Department of Agriculture-National Resources Conservation Service National Cartography and Geospatial Center, USDA-NRCS PRISM Climate Mapping Project-Precipitation, Mean monthly and annual precipitation digital files for the continental [CD-ROM], Ft. Worth, Tex., Dec. 1998. (Available at http://www.ocs.orst.edu/prism/)

Whipple, K. X., and G. E. Tucker, Dynamics of the stream-power river incision model: Implications for height limits of mountain ranges, landscape response timescales and research needs, *J. Geophys. Res.*, *104*, 17,661–17,674, 1999.

Whipple, K. X., and G. E. Tucker, Implications of sediment-flux-dependent river incision models for landscape evolution, *J. Geophys. Res.*, *107*(B2), 2039, doi:10.1029/2000JB000044, 2002.

Whipple, K. X., G. S. Hancock, and R. S. Anderson, River incision into bedrock: Mechanics and relative efficacy of plucking, abrasion and cavitation, *Geol. Soc. Am. Bull.*, *112*, 490–503, 2000.

Willgoose, G., R. L. Bras, and I. Rodriguez-Iturbe, A coupled channel network growth and hillslope evolution model: 1. Theory, *Water Resour. Res.*, 237–254, 1991.

Wohl, E., *Mountain Rivers*, *Water Resour. Monogr. Ser.*, vol. 14, 320 pp., AGU, Washington, D. C., 2000.

J. R. Barbour and M. T. Brandon, Department of Geology and Geophysics, Yale University, P.O. Box 208109, New Haven, CT 06520-8109, USA.

F. J. Pazzaglia, Department of Earth and Environmental Sciences, Lehigh University, 31 Williams Drive, Bethlehem, PA 18015, USA.

J. H. Tomkin, Department of Geology and Geophysics, Louisiana State University, Baton Rouge, LA 70803, USA. (tomkin@geol.lsu.edu)

S. D. Willett, Department of Earth and Space Sciences, University of Washington, Seattle, WA 98195, USA.